Submitted to *International Journal of Refractory Metals and Hard Materials*, Revised April 2020.

Spark plasma sinterability and dry sliding-wear resistance of WC densified with Co, Co+Ni, and Co+Ni+Cr

Aniss-Rabah Boukantar [a], Boubekeur Djerdjare [a],

Fernando Guiberteau [b], Angel L. Ortiz [b,*]

[a] Department of Materials Sciences, University of Sciences and Technology Houari Boumediene, Algiers, Algeria.

[b] Departamento de Ingeniería Mecánica, Energética y de los Materiales, Universidad de Extremadura, 06006 Badajoz, Spain.

Abstract

The spark plasma sinterability and the dry sliding-wear resistance of ultrafine-grained WC densified with ~16.7 vol.% of Co, Co+Ni, and Co+Ni+Cr, compositions equivalent to that of the typical WC-10wt.%Co, were investigated and compared critically. Firstly, it was found that the partial substitutions of Co by Ni or by Ni+Cr are detrimental for the pressureless ultrafast sinterability, but much more in the latter than the former case, attributable to the higher eutectic temperatures during liquid-phase sintering. However, it was also observed that, thanks to the auxiliary stress supplementing the sintering stresses, the ultrafast sinterability with pressure is affected by these partial substitutions either not at all (Co by Ni) or very little (Co by Ni+Cr), making it possible in all cases to obtain fully-dense WC cermets with almost no grain growth at the same spark plasma sintering temperature. And secondly, it was found that these cemented carbides are very resistant to dry sliding wear, but that WC-(Co+Ni+Cr) is markedly more so, attributable essentially to its greater hardness. This is due to wear occurring essentially by two-

body abrasion dominated by plastic deformation (ploughing), plus some oxidative wear with formation of tribo-oxidation layers that, although not entirely coherent, are nonetheless beneficial for the wear resistance.

Keywords: WC; spark plasma sintering; dry sliding wear; cemented carbides; metal binder.

* Corresponding author:

Angel L. Ortiz
Phone: +34 924289600 Ext: 86726
Fax: +34 924289601
E-mail: **alortiz@unex.es**

1. Introduction

WC with Co binder (WC-Co) is doubtless the most investigated, commercially developed, and industrially used of all cemented carbides. In particular, its excellent combination of hardness, toughness/ductility, strength, stiffness, and thermal shock resistance, to name but a few properties [1], makes WC-Co the choice material for the fabrication of a wide variety of wear-resistant parts [1]. Indeed, WC-Co is today essential in industrial applications as relevant as, for example, metal machining, mine excavation, oil drilling, and tunneling [2], among others.

Currently however, there is growing interest in the partial, and even total, substitution of the Co binder by other metals. The aim mainly is to optimize the properties, but there are other motivations as well (i.e., geopolitical, economic, safety, and environmental concerns) [1-3]. Ni has been of particular interest because it is cheaper and safer than Co, and offers greater ductility and oxidation/corrosion resistance [1-4]. WC-Ni is however softer and weaker than WC-Co [1], and is therefore used essentially only in those applications where oxidation/corrosion resistance is the primary concern [1]. WC-(Co+Ni), in which Co is partially, not totally, replaced by Ni, has a better balance of properties [5,6], and is therefore preferable to WC-Co and WC-Ni for many applications. Unfortunately however, not even WC-(Co+Ni) performs entirely satisfactorily under severe conditions of oxidation/corrosion, which has led to soaring interest in WC with Cr-containing binders [1]. Cr offers much greater oxidation/corrosion resistance while providing hardness [3,7,8], and is also cheaper and safer than Co. Unsurprisingly, WC-(Co+Ni+Cr), in which Co is partially replaced by Ni+Cr, is gaining attention within the hardmetals community [4,9-11] because Co+Ni+Cr binders are expected to offer a closer to optimal combination of sinterability, mechanical properties, and electrochemical behaviour.

There have however been very few studies on WC-(Co+Ni+Cr), and even these are very difficult, if not impossible, to compare with the numerous studies available for other most typical cemented carbides because they share no common experimental platform[I]. The present study contributes to palliating this paucity, and was aimed at comparing critically the spark plasma sinterability and the dry sliding-wear resistance of WC-(Co+Ni+Cr) relative to the widely-used WC-Co and WC-(Co+Ni). Spark plasma sintering (SPS)[II] was chosen because it is especially well-suited to producing the desired fine-grained microstructures for wear applications [1,12]. SPS is indeed an ultra-fast and energy-efficient sintering technique[III] whose application to cemented carbides is still relatively limited, but that it holds great promise in this field due to its potential to reduce the fabrication costs in relation for example to the widely-used sinter-HIP [1]. The choice of sliding wear was because it is common for these cemented carbides to operate under sliding contact.

2. Experimental procedure

The starting materials were commercially available powders of WC (Ref. 12482; 99.5% purity, d_{50}<1 μm), Co (Ref. 10455; 99.8% purity; d_{50}~1.6 μm), Ni (Ref. 10255; 99.9 purity, d_{50}~2.2-3.0 μm), and Cr (Ref. 41797; 99.2 purity, d_{50}<10 μm), all four purchased from Alfa Aesar (Germany), and used as-received. They were nonetheless characterized by X-ray diffractometry (XRD; D8 Advance, Bruker AXS, Germany), field-emission scanning electron

[I] Differences in the raw materials, densification methods/conditions, testing methods/conditions, etc.

[II] SPS essentially combines a direct heating of the die by the repeated application of high energy, low voltage, pulsed direct electrical current and high uniaxial mechanical pressure.

[III] SPS uses much shorter densification cycles than conventional pressureless sintering, hot-pressing, hot-isostatic pressing (HIP), and sinter-HIP. In particular, in SPS the heating/cooling ramps are one order of magnitude faster (hundreds vs tens of °C/min) and the holding times are one order of magnitude shorter (min vs h)), so that the typical SPS cycles last only ~15-30 min. The energy consumption is therefore drastically reduced, which translate into cost savings.

microscopy (FE-SEM; Quanta 3D, FEI, The Netherlands), and gas pycnometry (Stereopycnometer SPY-D160-E, Quantachrome Instruments, UK). The XRD patterns were collected over the 2θ angular range 20-90° using CuKα incident radiation, and were analysed with the PDF2 database to identity the crystalline phase(s) present. The FE-SEM images were acquired at 20 kV without metal coating, and were analysed by image analysis software to determine the particle sizes and morphology. The pycnometry measurements were done in triplicate using a calibrated cell (20 cm^3) and high-purity He (99.99%) regulated to 20 psi, and were used to compute the absolute densities. The Co, Ni, and Cr powders were also investigated by differential thermal analysis (DTA; STA 449 F3 Jupiter, Netzsch, Germany) to determine their melting points. The DTA curves were registered under an inert atmosphere of flowing Ar (50 ml/min) up to 1600°C, at a heating rate of 10°C/min.

Three powder batches were prepared, all designed to give cemented carbides with 83.307 vol.% WC plus 16.693 vol.% metal binder, this last with composition in vol.% of either (*i*) 100% Co, (*ii*) 80% Co and 20% Ni (i.e., with partial substitution of Co by Ni), or (*iii*) 40% Co, 20% Ni, and 40% Cr (i.e., with partial substitution of Co by Ni+Cr). These vol.% of WC and binder are not arbitrary, but correspond to the typical WC-10wt.%Co. The powder mixtures of WC-16.693Co, WC-(13.354Co+3.339Ni), and WC-(6.677Co+3.339Ni+6.677Cr) were obtained by first combining the WC, Co, Ni, and Cr powders in appropriate proportions as listed in Table 1, then wet-mixing them with abundant methanol (~100 g/l), next mechanically stirring the slurries at room temperature for 24 h using a rotavap, and lastly drying the slurries at ~70°C under continuous stirring in the rotavap. The resulting powder mixtures were also characterized by XRD and DTA.

Two types of SPS (HP-D-10, FCT Systeme GmbH, Germany) tests were implemented – dilatometric or densification. In the former, the three powder mixtures were individually spark plasma sintered (SPS-ed) under non-isothermal heating (ramp of 100°C/min) up to 1700°C (without soaking time) at electrical-contact pressure (~4 MPa). The WC-16.693Co powder mixture was also SPS-ed non-isothermally up to 1400°C under 50 MPa pressure (applied at 300°C). In the latter, the powder mixtures were individually SPS-ed under isothermal heating (ramp of 100°C/min) at 1150°C, 1200°C, and 1250°C for 5 min, under 50 MPa pressure (applied at 300°C). All SPS cycles were conducted in dynamic-vacuum atmosphere, and had a final segment (of 2 min duration) of ultrafast cooling to room temperature and load release. Also, during each SPS cycle the shrinkage and shrinkage-rate curves were logged, which were then corrected for the expansion of the graphite parts before their subsequent analysis.

The SPS-ed cemented carbides were ground and polished to a 0.25-µm finish using conventional ceramographic methods, and were characterized by XRD and FE-SEM. They were also characterized mechanically by Vickers indentation tests (MV-1, Matsuzawa, Japan) at 30 N load (P) to determine their hardness (H_V) and fracture toughness (K_{IC}) using the following expressions [13-16]:

$$H_V = \frac{2P}{d^2}$$

$$K_{IC} = 0.0889\sqrt{\frac{H_V P}{\sum_{i=1}^{4} c_i}}$$

where d is the average diagonal of the residual indent and c is the length of each of the four Palmqvist cracks emanating from the corners of the Vickers imprint. The Vickers tests were performed in quintuplicate.

The wear tests were conducted with a pin-on-disk tribometer (THT1000, Anton Paar, Switzerland), using ultrahard diamond-coated SiC balls (Dball G10, Nova Diamant, UK) of 6.02 mm diameter as pins to ensure wear of the cemented carbides only. The wear tests were performed in duplicate at room temperature in dry conditions (without lubricant), under normal contact load of 60 N, linear sliding speed of 10 cm/s, track radius of 2 mm, and total sliding distance of 2000 m. At the conclusion of the wear tests, the residual tracks on the cemented carbides were measured by optical profilometry (Profilm 3D, Filmetric, USA) to evaluate the worn volumes, and the damage within the wear tracks was observed by optical microscopy and FE-SEM. Energy-dispersive X-ray spectrometry (EDS) analyses were also conducted at different locations both inside (centre and edge) and outside the wear tracks to elucidate possible changes in surface chemical composition during wear.

3. Results and Discussion

3.1. Comparative study of spark-plasma sinterability

3.1.1. Characterization of the starting powders

Figures 1 and 2 show representative FE-SEM images and the XRD patterns, respectively, of the four starting powders. Clearly, the WC powder contains equiaxed particles of submicrometre size (Fig. 1A), and is essentially α-WC (hcp) with some β-W_2C (hcp) as minor phase (Fig. 2A). The presence of β-W_2C in trace amounts is because the WC powder is slightly carbon deficient (W:C weight ratio of ~15.42 instead of 15.31). The Co powder comprises micrometre worm-like particles formed by intergrowths of submicrometre particles (Fig. 2B), and is a combination of both α-Co (hcp) and β-Co (fcc) (Fig. 2B). The Ni powder contains micrometre equiaxed agglomerates of primary ultrafine particles (Fig. 1C), and is formed by β-Ni (fcc) exclusively (Fig. 2C). Lastly, the Cr powder comprises micrometre agglomerates of

flattened-like submicrometre particles (Fig. 1D), and contains only β-Cr (bcc) (Fig. 2D). According to the He-pycnometry, the WC, Co, Ni, and Cr powders have absolute densities of 15.572(6) g/cm³, 8.635(14) g/cm³, 8.735(18) g/cm³, and 7.046(5) g/cm³, respectively.

Figure 3 shows the DTA curves of the Co, Ni, and Cr starting metal powders. Co and Ni exhibit an endothermic event at ~1493°C and 1460°C, respectively, attributable to their melting (the reference melting temperatures for Co and Ni are ~1495°C and 1455°C, respectively [17]). On the contrary, Cr does not exhibit any thermal event because it melts at ~1907°C [17], and the DTA tests reached only 1600°C (which is the upper-limit temperature of the thermobalance used).

3.1.2. Dilatometric SPS tests

Figure 4 shows the densification curves as a function of temperature up to 1700°C obtained from the pressureless dilatometric SPS tests (i.e., under only electrical-contact pressure). It is evident that the partial substitutions of Co by Ni and especially by Ni+Cr are detrimental in terms of pressureless sinterability because WC-16.693Co exhibits the fastest densification kinetics and the greatest ultimate densification, closely followed by WC-(13.354Co+3.339Ni), and far behind by WC-(6.677Co+3.339Ni+6.677Cr). Thus for example, WC-16.693Co entered the intermediate and final sintering regimes [18][IV] at slightly lower temperatures (~1272°C and 1305°C, respectively) than WC-(13.354Co+3.339Ni) (~1295°C and 1332°C, respectively), and this latter in turn did so at notably lower temperatures than WC-(6.677Co+3.339Ni+6.677Cr) (~1342°C and 1462°C, respectively). Indeed, both WC-16.693Co and WC-(13.354Co+3.339Ni) are already very dense (~95%) at 1360°C, a temperature at which

[IV] The intermediate sintering regime is that during which the pore distribution transitions from open porosity to closed porosity, and is typically taken to begin at ~70% relative density. The final sintering regime is that during which the closed porosity is eliminated, and is normally taken to start at ~90% relative density.

WC-(6.677Co+3.339Ni+6.677Cr) is very porous (~74%). Also, at 1700°C WC-16.693Co is fully dense, WC-(13.354Co+3.339Ni) near-fully dense (~97.7%), and WC-(6.677Co+3.339Ni+6.677Cr) only very dense (~96.6%).

Figure 5 shows the corresponding pressureless shrinkage-rate curves. The three powder mixtures exhibit an abrupt peak of shrinkage rate attributable to the expected liquid-phase sintering [4,19,20], i.e., to the formation of liquid phase that rapidly spreads and wets the WC particles, filling pores and promoting particle rearrangement and solution-reprecipitation [18,21]. Thus, the composition of the metal binder did not affect the densification mechanism, but only the densification kinetics. The shrinkage-rate curves also confirm that WC-16.693Co is more sinterable than WC-(13.354Co+3.339Ni), and much more so than WC-(6.677Co+3.339Ni+6.677Cr), because the densification peak is far more intense (~3.84 mm/min vs. ~2.62-2.82 mm/min) and occurred at a lower temperature (~1273°C vs ~1293°C). This reflects that the partial substitutions of Co by Ni and by Ni+Cr shifted the eutectic points towards higher temperatures [3,4]. Distinctively, the densification peak of WC-(6.677Co+3.339Ni+6.677Cr) falls slowly, not abruptly as in WC-16.693Co and WC-(13.354Co+3.339Ni), thus reflecting that its densification is much more gradual.

Figure 6 shows the DTA curves of the three powder mixtures confirming the above conclusions. It is clear that WC-16.693Co exhibits an endothermic event at ~1357°C, attributable to the formation of eutectic liquid because the Co melting point is well above at ~1493°C (Fig. 3). The formation of eutectic liquid in WC-(13.354Co+3.339Ni) occurred ~25°C above, at ~1382°C, again well below the 1460°C and 1493°C of the Ni and Co melting points, respectively (Fig. 3). This temperature difference is indeed the same as that of the corresponding shrinkage-

rate peaks (~20°C above in WC-(13.354Co+3.339Ni))[V]. Finally, the formation of eutectic liquid in WC-(6.677Co+3.339Ni+6.677Cr) occurred essentially at the same temperature as in WC-(13.354Co+3.339Ni), but more abruptly and over a broader temperature range. The same is the case with WC-(Ni+Cr) for which earlier DTA results have revealed that the eutectic reaction is replaced by a melting range [4]. Therefore, both the present DTA analyses and the SPS curves indicate that the partial substitutions of Co by Ni and by Ni+Cr increased the eutectic temperatures.

Interestingly, the shrinkage-rate curves show that it is impractical to use SPS temperatures above ~1350°C, especially because SPS with pressure will increase the driving force for densification by supplementing the sintering stresses with an auxiliary stress [18]. In this sense, Fig. 7 shows the shrinkage-rate curve corresponding to the dilatometric SPS test performed on WC-16.693Co up to 1400°C under 50 MPa pressure, indicating (*i*) that the densification peak occurs ~30°C below at ~1245°C-1250°C, (*ii*) that there is now marked densification between ~1150°C and ~1250°C, and (*iii*) that above ~1250°C the densification rate drops abruptly. The shrinkage-rate peak is less intense (~2.53 mm/mm vs ~3.84 mm/min), but this is simply because the sintering force declines to zero as porosity is eliminated [18]. Therefore, SPS of the three types of cemented carbides will be performed at 1150°C, 1200°C, and 1250°C, because above 1250°C there will be no further densification but marked microstructural coarsening and higher risk of liquid spillage within the graphite dies.

[V] The DTA and SPS temperatures are not however directly comparable (different heating schedules, temperature within the graphite die greater than measured by the optical pyrometer, pressure of ~4 MPa in SPS but not in DTA, etc.).

3.1.3. Densification SPS tests

Figure 8 shows the densification curves as a function of temperature that were obtained from the SPS tests with isothermal soaking at 1150°C, 1200°C, and 1250°C for 5 min under 50 MPa pressure. It is clear that these curves all have the same general shape, with two stretches during the non-isothermal heating regime, one of very little densification and the other of accelerated densification, plus a third stretch of gradual densification during the isothermal heating regime. This is the type of curve already observed for other advanced ceramics [19,22-29]. It is also clear that the degree of densification increased with increasing SPS temperature, attributable to diffusion's being a thermally-activated process obeying an Arrhenius-type law [30]. More interestingly, unlike the pressureless sintering, the partial substitution of Co by Ni did not affect the sinterability with pressure, while that of Co by Ni+Cr had only a minor influence. Thus for example, WC-16.693Co and WC-(13.354Co+3.339Ni) reached the intermediate and final sintering regimes at the same temperatures of ~1190°C and 1245°C, respectively, while WC-(6.677Co+3.339Ni+6.677Cr) did so at ~1232°C (i.e., only ~42°C above) and after ~10 s at 1250°C (i.e., only ~13 s after), respectively. The ultimate densifications reached at 1200°C and 1250°C are also the same, with 1250°C being the optimal SPS temperature in the three cases (100% densification). While there were greater differences at 1150°C, they are irrelevant because these cemented carbides are very porous.

Finally, as expected, the application of pressure benefited the sinterability, but more markedly with WC-(6.677Co+3.339Ni+6.677Cr). Thus for example, the reduction in the onset temperature of the final sintering regime was by ~212°C for WC-(6.677Co+3.339Ni+6.677Cr), but only by ~60°C for WC-16.693Co and ~87°C for WC-(13.354Co+3.339Ni). This is not a

surprise because it is well established that the lower the intrinsic sinterability the greater the benefit of pressure-assisted sintering [18,31,32].

3.1.4. Microstructure of the SPS-ed cemented carbide

Figure 9 shows the XRD patterns of the nine cemented carbides fabricated, together with those of the corresponding powder mixtures. It is clear that WC-16.693Co SPS-ed at 1150°C and 1200°C both contain α-WC (major phase), β-Co(W,C) (minor phase), and Co_3W_3C (minor phase), while that SPS-ed at 1250°C contains only the first two. Both β-Co(W,C) and Co_3W_3C formed during SPS because they do not appear in the XRD pattern of the WC-16.693Co powder mixture. β-Co(W,C) is an fcc solid solution of W and C in β-Co with a larger lattice parameter, whereas Co_3W_3C is a metastable sub-stoichiometric ternary carbide called η-phase (M_6C, where M=metal). M_6C is undesirable because, being hard, it reduces the toughness of cemented carbides [1,33]. However, none of the SPS-ed WC-16.693Co contain β-W_2C, β-Co, or α-Co. It therefore seems that, because the actual temperature of the powder compact within the graphite die is greater than that measured by the optical pyrometer (focused inside the upper graphite punch in the vicinity of, but not at, the sample), SPS of WC-16.693Co at 1150°C and 1200°C fell within the three-phase region WC+η+liquid of the pseudo-binary phase diagram WC-Co [34], whereas SPS at 1250°C fell within the two-phase region WC+liquid. The ultrafast cooling applied in SPS then "froze" the phases present at these SPS temperatures, with the liquid solidification giving crystalline β-Co(W,C). All SPS-ed WC-(13.354Co+3.339Ni) and WC-(6.677Co+3.339Ni+6.677Cr), however, contain α-WC (major phase), β-M(W,C) (minor phases), and M_6C (minor phases). Consequently, SPS of these cemented carbides always fell within the three-phase region WC+η+liquid, attributable to the partial substitutions of Co by Ni and by Ni+Cr increasing the eutectic temperatures.

Figure 10 shows representative secondary-electron FE-SEM images of the nine cemented carbides fabricated, whereas by way of example Fig. 11 shows the equivalent backscattered-electron FE-SEM image for one of these cemented carbides. It can be seen that they all have ultrafine-grained microstructures, with submicrometre average grain sizes (< 1 μm). Also, it is clear that the none of the cemented carbides SPS-ed at 1150°C are dense, and that WC-(6.677Co+3.339Ni+6.677Cr) is the most porous. Indeed, FE-SEM observations at lower magnifications, such as those shown in Fig. 12, demonstrate that, unlike WC-16.693Co and WC-(13.354Co+3.339Ni), WC-(6.677Co+3.339Ni+6.677Cr) SPS-ed at 1150°C has an inhomogeneous microstructure with both well-densified regions and highly-porous regions, indicating that it reached only the middle stage of the intermediate sintering regime. SPS at 1200°C and 1250°C, however, in the three cases resulted in near-fully dense and fully dense cemented carbides, respectively. Also, the complete densification occurred with little grain growth, attributable to the short duration of the SPS cycles which lasted for less than 20 min (total time). This minimized the events of solution-reprecipitation responsible for microstructural coarsening during liquid-phase sintering [18,21], and resulted in very homogeneous microstructures with little dispersion in the grain sizes.

3.2. Comparative study of dry sliding-wear resistance

3.2.1. Hardness and fracture toughness

Figure 13A shows the hardness (H_V) determined by Vickers indentation for the nine cemented carbides fabricated. It is clear that H_V increased with increasing SPS temperature, first very markedly (by ~5.5 GPa for WC-16.693Co and WC-(13.354Co+3.339Ni), and by ~14 GPa for WC-(6.677Co+3.339Ni+6.677Cr)), and then only slightly (by ~0.6 GPa in all three cases). Therefore, it is clearly evident that the hardness of these cemented carbides correlates inversely

with their porosity, increasing with increases in their degree of densification. It can also be seen that well-densified WC-(6.677Co+3.339Ni+6.677Cr) is harder (by ~3 GPa) than WC-16.693Co and WC-(13.354Co+3.339Ni). If at all, WC-16.693Co would be only marginally harder (by ~0.5 GPa) than WC-(13.354Co+3.339Ni). Interestingly, WC-(6.677Co+3.339Ni+6.677Cr) reached a notably high hardness of ~20-21 GPa, whereas WC-16.693Co and WC-(13.354Co+3.339Ni) reached the hardness of ~17-18 GPa expected for submicrometre-grained WC-based cemented carbides with such a binder content [1,35,36] including those fabricated by sinter-HIP [37].

Figure 13B shows the fracture toughness (K_{IC}) also determined by Vickers indentation for the cemented carbides SPS-ed at 1200°C and 1250°C.[VI] It can be seen that they are quite tough (~9.5-13 MPa·m$^{0.5}$), and that, although just slightly, K_{IC} increased with increasing SPS temperature. WC-16.693Co seems slightly tougher than WC-(13.354Co+3.339Ni), and both are much tougher than WC-(6.677Co+3.339Ni+6.677Cr). Also, WC-16.693Co is as tough as its counterpart fabricated by sinter-HIP [37]. Thus, contrarily to the expectation, partial substitution of Co by Ni did not result in enhanced toughness, which is attributable to the undesirable presence of brittle M_6C phases in the microstructure of WC-(13.354Co+3.339Ni). The same is the case for the partial substitution of Co by Ni+Cr, together with the fact that Cr is intrinsically less ductile than Co.

3.2.2. Dry sliding-wear tests

Figure 14 shows the coefficient of friction (CoF) registered as a function of sliding distance for the cemented carbides SPS-ed at 1250°C, chosen for the comparative tribological tests because they are fully dense and also the hardest and toughest. Clearly, there is an initial

[VI] It was not measured for the cemented carbides SPS-ed at 1150°C simply because the residual porosity will artificially overestimate the true toughness.

running-in stage (~250 m of sliding), and then a steady-state stage in which the CoFs stabilized at ~0.06-0.08. This low friction is very desirable because it indicates little resistance to sliding, and then, foreseeably, little wear. However, these CoFs are strikingly low for dry sliding contact, even considering that the counter-ball is of high-grade SiC coated with high-quality microcrystalline CVD diamond. Indeed, CoFs lower than 0.1 are typical of lubricated sliding contacts [38,39], which suggests that there was a lubrication mechanism.

Figure 15 shows representative optical images of the residual wear tracks in the three cemented carbides after 2000 m of sliding. As expected from the low CoFs, there was little wear because the wear tracks are fairly narrow (<250 μm) and look relatively shallow. Certainly, the worn volumes calculated by optical profilometry are only ~$4.78 \cdot 10^{-4}$ mm³, $5.53 \cdot 10^{-4}$ mm³, and $2.67 \cdot 10^{-4}$ mm³ for WC-16.693Co, WC-(13.354Co+3.339Ni), and WC-(6.677Co+3.339Ni+6.677Cr), respectively. This corresponds to specific wear rates (SWRs) as low as ~$3.98 \cdot 10^{-9}$ mm³/(N·m), ~$4.61 \cdot 10^{-9}$ mm³/(N·m), and ~$2.22 \cdot 10^{-9}$ mm³/(N·m), respectively. These SWRs are of the order of magnitude of only 10^{-9} mm³/(N·m), and are thus indicative of just mild wear despite the wear tests having been performed in dry conditions [40]. However, it is also clear that WC-(6.677Co+3.339Ni+6.677Cr) was comparatively much more wear resistant (~$4.50 \cdot 10^{8}$ (N·m)/mm³) than WC-16.693Co (~$2.51 \cdot 10^{8}$ (N·m)/mm³) and WC-(13.354Co+3.339Ni) (~$2.17 \cdot 10^{8}$ (N·m)/mm³). It is thus reasonable to think that wear was dominated by plastic deformation, not by fracture, because WC-(6.677Co+3.339Ni+6.677Cr) is indeed the hardest and least tough of these three cemented carbides.

3.2.3. Wear damage and mechanisms

Figure 16 show representative low-magnification FE-SEM images of the residual wear tracks in the three cemented carbides after 2000 m of sliding. It is clear that tribolayers were

formed during wear. As seen in the series of higher-magnification FE-SEM images shown by way of example in Fig. 17, the tribolayers are not, however, entirely coherent[VII]. For instance, they have variable thicknesses (Figs. 17A-C), and show evidence of localized cracking (Figs. 17A and D), delamination (Fig. 17D), and spalling (Fig. 17E). Interestingly, the EDS spectra shown in Fig. 18 revealed that the wear tracks contain much more oxygen than the passivating layers spontaneously developed outside at the unworn surfaces[VIII]. The tribolayers do not contain more carbon, however, which rules out their formation by mass transfer from the diamond counter-ball. Indeed, the tribolayers are surface oxides formed *in situ* during the tribological tests (presumably during the running-in stage) due to the frictional heating generated under air atmosphere. It therefore seems that there was some oxidative wear, but also that the tribo-oxidation layers were beneficial for the wear resistance because, despite their non-uniform thickness and localized defects, they are well-adhered and cover most part of the contact surface and therefore they (*i*) prevented direct contact between the cemented carbide and the counter-ball thus separating asperity contacts and (*ii*) lubricated the contact thus reducing the friction (as inferred from the low CoFs in Fig. 13) due to their lower shear strength [38].

Figure 19 shows representative FE-SEM images of the interior of the residual wear tracks in the three cemented carbides after 2000 m of sliding. It is clear that the wear damage consists of superficial scratches, in the form of very shallow grooves running parallel to the sliding direction. This is indicative of abrasion. Also, the worn surfaces are still quite smooth and remain intact overall, without evidence of noticeable pits. This rules out ostensible fracture. As seen in the higher-magnification FE-SEM images shown by way of example in Fig. 20, there was only a

[VII] A tribolayer is said to be coherent if it is well-adhered, is homogeneous in composition and uniform in thickness, and is defect-free with no signs of cracking, delamination, or spalling.

[VIII] WC, M_6C, and β-M(W,C) are non-oxide compounds, and therefore they passivate naturally in air.

very limited pullout of material here and there, but no wholesale material removal. There is then no wear debris entrapped between the two sliding surfaces that act as abrasives. This is true both in areas where tribo-oxidation layers are evident (Fig. 20A) and where they are not (Fig. 20B). Thus, it is clear that there was mechanical wear by abrasion dominated by plastic deformation, not by fracture. This was two-body abrasion because the absence of sufficient wear debris excluded the occurrence of three-body abrasion, leaving sliding contact of surface asperities as the cause of wear. In addition, abrasive wear took place by ploughing [38] because there is no evidence of wedge formation or micro-cutting (Fig. 20C).

The microstructural observations of the wear tracks thus indicate that these cemented carbides wore by a combination of oxidative and mechanical wear, but with the latter predominating over the former because the wear resistance correlated with the hardness and not with the oxidation resistance. For example, WC-16.693Co was more wear resistant than WC-(13.354Co+3.339Ni) despite its inferior oxidation resistance (confirmed by EDS).[IX] Conversely, the order of wear resistance followed the order of hardness, as predicted by the classical Archard's law of plasticity-dominated wear [41,42]. In any case, the severity of the wear was very mild in all three cases, attributable to the high hardness of these cemented carbides and to the extra anti-wear protection provided by the tribo-oxidation layers.

To conclude, it is important to mention that, although the wear studies may be hard to extrapolate, it is at least clear that the still little-investigated WC-(Co+Ni+Cr) cemented carbides hold great promise for tribological applications. Given their greater safeness and cheapness, they therefore deserve further studies aimed at critically examining their wear resistance under a

[IX] The oxygen contents determined by EDS for the passivating layers on WC-16.693Co, WC-(13.354Co+3.339Ni), and WC-(6.677Co+3.339Ni+6.677Cr) are ~8.4(9), 5.2(6), and 0.2(1) at.%, respectively. As expected, the partial substitution of Co by Ni therefore increased the oxidation resistance, and that of Co by Ni+Cr did so much more.

wider set of testing methods and conditions. Also, future studies are also needed aimed at investigating their densification by conventional pressureless sintering.

4. Conclusions

We have taken the composition of the widely-recognized WC-10wt.%Co cemented carbide and replaced partially the Co binder by Ni or by Ni+Cr while maintaining the metal binder vol.% constant, then investigating its effect on the spark-plasma sinterability and dry sliding-wear resistance. Based on the experimental results and analyses, the following conclusions can be drawn:

1. Partial substitutions of Co by Ni and by Ni+Cr reduce (slightly the former and considerably the latter) the pressureless ultrafast sinterability of WC, attributable to the greater temperatures required for the formation of low-viscosity eutectic liquid.
2. The metal binder (Co, Co+Ni, or Co+Ni+Cr) does not condition the ultrafast sinterability under the typical pressures applied in conventional SPS. This is because the auxiliary stress facilitates the densification even for more viscous and less abundant liquid phases.
3. Fully-dense WC-(Co+Ni+Cr) is markedly harder (~21 GPa, ~3-4 GPa more) than both WC-Co and WC-(Co+Ni), while still preserving a fracture toughness above 9 $MPa \cdot m^{0.5}$. This is a good combination of mechanical properties for very many structural applications.
4. WC-(Co+Ni+Cr) has excellent intrinsic dry sliding-wear resistance that comparatively exceeds those of WC-Co and WC-(Co+Ni) by a factor of two, attributable to its superior hardness. Nonetheless, WC-Co and WC-(Co+Ni) also exhibit very mild wear (SWRs of 10^{-9} $mm^3/(N \cdot m)$).
5. Wear of these cemented carbides under dry sliding contact in air occurs principally by

two-body abrasion dominated by plastic deformation (specifically, ploughing), with some oxidative wear. The formation of tribo-oxidation layers, although not entirely coherent, is nonetheless beneficial for the wear resistance.

Acknowledgements. This work was supported by the Ministerio de Economía y Competitividad (Government of Spain) and FEDER Funds under the Grant nº MAT2016-76638-R. Financial support from the Junta de Extremadura under the Grant nº GR18149, also co-financed with FEDER Funds, is gratefully acknowledged as well.

References

1. J. García, V. Collado Ciprés, A. Blomqvist, B. Kaplan, Cemented carbide microstructures: a review, Int. J. Refract. Met. Hard Mat. 80 (2019) 40–68.
2. R.F. Santos, A.M. Ferro Rocha, A.C. Bastos, J.P. Cardoso, F. Rodrigues, C.M. Fernandes, J. Sacramento, M.G.S. Ferreira, A.M.R. Senos, C. Fonseca, M.F. Vieira, L.F. Malheiros, Microstructural characterization and corrosion resistance of WC-Ni-Cr-Mo composite – The eff ect of Mo, Int. J. Refract. Met. Hard Mat. 86 (2020) 105090.
3. C.M. Fernandes, A.M.R. Senos, Cemented carbide phase diagrams: a review, Int. J. Refract. Met. Hard Mat. 29 (2011) 405–418.
4. M. Aristizabal, N. Rodriguez, F. Ibarreta, R. Martinez, J.M. Sanchez, Liquid phase sintering and oxidation resistance of WC–Ni–Co–Cr cemented carbides, Int. J. Refract. Met. Hard Mat. 28 (2010) 516–522.
5. X. Zhang, J. Zhou, C. Liu, K. Li, W. Shen, Z. Lin, Z. Li, Y. He, N. Lin, Effects of Ni addition on mechanical properties and corrosion behaviors of coarse-grained WC-10(Co,Ni) cemented carbides, Int. J. Refract. Met. Hard Mat. 80 (2019) 123–129.
6. W. Su, Y. Sun, J. Liu, J. Feng, J. Ruan, Effects of Ni on the microstructures and properties of WC–6Co cemented carbides fabricated by WC–6(Co,Ni) composite powders, Ceram. Int. 41 [2 Part B] (2015) 3169–3177.
7. J.E. Cho, S.Y. Hwang, K.Y. Kim, Corrosion behavior of thermal sprayed WC cermet coatings having various metallic binders in strong acidic environment, Surf. Coat. Technol. 200 (2006) 2653–2662.
8. T.W. Penrice, Alternative binders for hard metals, Carbide Tool J. 20 [4] (1988) 12–15.

9. B. Lopez Ezquerra, L. Lozada, H. van den Berg, M. Wolf, J.M. Sánchez, Comparison of the thermal shock resistance of WC based cemented carbides with Co and Co-Ni-Cr based binders, Int. J. Refract. Met. Hard Mat. 72 (2018) 89–96.
10. M. Aristizabal, J.M. Sanchez, N. Rodriguez, F. Ibarreta, R. Martinez, Comparison of the oxidation behaviour of WC–Co and WC–Ni–Co–Cr cemented carbides, Corrosion Science 53 (2011) 2754–2760.
11. M. Aristizabal, L.C. Ardila, F. Veiga, M. Arizmendi, J. Fernandez, J.M. Sánchez Moreno, Comparison of the friction and wear behaviour of WC–Ni–Co–Cr and WC–Co hardmetals in contact with steel at high temperatures, Wear 280–281 (2012) 15–21.
12. X. Wang, N.P. Padture, H. Tanaka, A.L. Ortiz, Wear-resistant ultra-fine-grained ceramics, Acta Mater 53 (2005) 271–277.
13. D.G. Green, An Introduction to the Mechanical Properties of Ceramics, Cambridge University Press, Cambridge, UK, 1998.
14. D.K. Shetty, I.G. Wright, P.N. Mincer, A.H. Clauer, Indentation fracture of WC–Co cermets, J. Mat. Sci. 20 (1985) 1873–1882.
15. A.M. Soleimanpour, P. Abachi, A. Simchi, Microstructure and mechanical properties of WC–10Co cemented carbide containing VC or (Ta,Nb)C and fracture toughness evaluation using different models, Int. J. Refract. Met. Hard Mat. 31 (2012) 141–146.
16. T.A. Fabijanić, D. Ćorić, M. Šnajdar Musa, M. Sakoman, Vickers indentation fracture toughness of near-nano and nanostructured WC-Co cemented carbides, Metals 7 (2017) 143.
17. R.C. Weast (Editor), Handbook of Chemistry and Physics, 59th Edition, CRC Press Inc, Florida, 1978.
18. R.M. German, Sintering theory and practice, Wiley, New York, 1996.

19. C. Ojalvo, F. Guiberteau, A.L. Ortiz, Fabricating toughened super-hard B_4C composites at lower temperature by transient liquid-phase assisted spark plasma sintering with $MoSi_2$ additives, J. Eur. Ceram. Soc. 39 [9] (2019) 2862–2873.
20. A.L. Ortiz, C.A. Galán, O. Borrero-López, F. Guiberteau, Highly sliding-wear resistant B_4C composites fabricated by spark-plasma sintering with Ti–Al additives, Scripta Mater. 177 (2020) 91–95.
21. R.M. German, Liquid phase sintering, Plenum Press, New York, US, 1985.
22. V. Zamora, A.L. Ortiz, F. Guiberteau, M. Nygren, Crystal-size dependence of the spark-plasma-sintering kinetics of ZrB_2 ultra-high-temperature ceramics, J. Eur. Ceram. Soc. 32 [2] (2012) 271–276.
23. B. Núñez-González, A.L. Ortiz, F. Guiberteau, M. Nygren, Improvement of the spark-plasma-sintering kinetics of ZrC by high-energy ball-milling, J. Am. Ceram. Soc. 95 [2] (2012) 453–456.
24. V. Zamora, A.L. Ortiz, F. Guiberteau, M. Nygren, Spark-plasma sintering of ZrB_2 ultra-high-temperature ceramics at lower temperature via nanoscale crystal refinement, J. Eur. Ceram. Soc. 32 [10] (2012) 2529–2536.
25. V. Zamora, A.L. Ortiz, F. Guiberteau, M. Nygren, On the enhancement of the spark-plasma-sintering kinetics of ZrB_2–SiC powder mixtures subjected to high-energy coball-milling, Ceram. Int. 39 [4] (2013) 4191–4204.
26. B. Núñez-González, A.L. Ortiz, F. Guiberteau, M. Nygren, Spark-plasma-sintering kinetics of ZrC–SiC powder mixtures subjected to high-energy co-ball-milling, Ceram. Int. 39 [8] (2013) 9691–9697.

27. A. Motealleh, A.L. Ortiz, O. Borrero-López, F. Guiberteau, Effect of hexagonal-BN additions on the sliding-wear resistance of fine-grained α-SiC densified with $Y_3Al_5O_{12}$ liquid phase by spark-plasma sintering, J. Eur. Ceram. Soc. 34 [3] (2014) 565–574.
28. V. Zamora, M. Nygren, F. Guiberteau, A.L. Ortiz, Effect of graphite addition on the spark-plasma sinterability of ZrB_2 and ZrB_2–SiC ultra-high-temperature ceramics, Ceram. Int. 40 [7 Part B] (2014) 11457–11464.
29. V.M. Candelario, R. Moreno, Z. Shen, F. Guiberteau, A.L. Ortiz, Liquid-phase assisted spark-plasma sintering of SiC nanoceramics and their nanocomposites with carbon nanotubes, J. Eur. Ceram. Soc. 37 (5) (2017) 1929–1936.
30. D.R. Poirier, G.H. Geiger, Transport phenomena in materials processing, Pennsylvania, USA: the minerals, metals and materials society, 1998.
31. Z.A. Munir, U. Anselmi-Tamburini, M. Ohyanagi, The effect of electric field and pressure on the synthesis and consolidation of materials: a review of the spark plasma sintering method, J. Mat. Sci. 41 [3] (2006) 763–777.
32. R.M. German, Sintering: from empirical observations to scientific principles, Butterworth-Heinemann (Elsevier), Woburn, US, 2014.
33. C.M. Fernandes, A.M.R. Senos, M.T. Vieira, Control of eta carbide formation in tungsten carbide powders sputter-coated with (Fe/Ni/Cr), Int. J. Refract. Met. Hard Mat. 25 (2007) 310–317.
34. G.S. Upadhyaya, Materials science of cemented carbides: an overview, Mater. Design 22 (2001) 483–489.

35. G. Gille, J. Bredthauer, B. Gries, B. Mende, W. Heinrich, Advanced and new grades of WC and binder powder – their properties and application, Int. J. Refract. Met. Hard Mat. 18 [2-3] (2000) 87–102.
36. G. Gille, B. Szesny, K. Dreyer, H. van den Berg, J. Schmidt, T. Gestrich, G. Leitner, Submicron and ultrafine grained hardmetals for microdrills and metal cutting inserts, Int. J. Refract. Met. Hard Mat. 20 [1] (2002) 3–22.
37. C.B. Wei, X.Y. Song, J. Fu, X.M. Liu, Y. Gao, H.B. Wang, S.X. Zhao, Microstructure and properties of ultrafine cemented carbides—Differences in spark plasma sintering and sinter-HIP, Mat. Sci. Eng. A 552 (2012) 427–433.
38. B. Bhushan, Modern tribology handbook, CRC Press, Boca Raton, USA, 2001.
39. K. Kato, Tribology of ceramics, Wear 136 [1] (1990) 117–133.
40. G.W. Stachowiak, A.W. Batchelor, Engineering tribology, Butterworth-Heinemann (Elsevier), Oxford, UK, 2005.
41. J.F. Archard, Single contacts and multiple encounters, J. Appl. Phys. 32 [8] (1961) 1420–1425.
42. E. Rabinowicz, Friction and wear of materials, John Wiley and Sons, Hoboken, USA, 1965.

Figure Captions

Figure 1. FE-SEM micrographs of the individual starting powders of (A) WC, (B) Co, (C) Ni, and (D) Cr.

Figure 2. XRD patterns of the individual starting powders of WC, Co, Ni, and Cr. Peak assignations with the phase identification are included.

Figure 3. DTA curves of the individual starting powders of Co, Ni, and Cr used as metal binders, measured as a function of the temperature in the range 100°C-1600°C.

Figure 4. Densification curves as a function of temperature up to 1700°C logged during the dilatometric SPS tests for the powder mixtures of WC-16.693Co, WC-(13.354Co+3.339Ni), and WC-(6.677Co+3.339Ni+6.677Cr).

Figure 5. Shrinkage-rate curves as a function of temperature up to 1700°C logged during the dilatometric SPS tests for the powder mixtures of WC-16.693Co, WC-(13.354Co+3.339Ni), and WC-(6.677Co+3.339Ni+6.677Cr).

Figure 6. DTA curves of the powder mixtures of WC-16.693Co, WC-(13.354Co+3.339Ni), and WC-(6.677Co+3.339Ni+6.677Cr), measured as a function of the temperature in the range 100°C-1600°C.

Figure 7. Shrinkage-rate curves as a function of temperature up to 1400°C logged during both the dilatometric and densification SPS tests for the powder mixture of WC-16.693Co.

Figure 8. Densification curves as a function of temperature logged during the densification SPS tests with target temperatures of 1150°C, 1200°C, and 1250°C for the powder mixtures of (A) WC-16.693Co, (B) WC-(13.354Co+3.339Ni), and (C) WC-(6.677Co+3.339Ni+6.677Cr).

Figure 9. XRD patterns of the cemented carbides of (A) WC-16.693Co, (B) WC-(13.354Co+3.339Ni), and (C) WC-(6.677Co+3.339Ni+6.677Cr) SPS-ed at 1150°C, 1200°C, and 1250°C, together with the XRD patterns of the corresponding powder mixtures. Peak assignations with the phase identification are included.

Figure 10. FE-SEM micrographs of the nine cemented carbides fabricated: (A) WC-16.693Co, (B) WC-(13.354Co+3.339Ni), and (C) WC-(6.677Co+3.339Ni+6.677Cr) SPS-ed at 1150°C; (D) WC-16.693Co, (E) WC-(13.354Co+3.339Ni), and (F) WC-(6.677Co+3.339Ni+6.677Cr) SPS-ed at 1200°C; and (G) WC-16.693Co, (H) WC-(13.354Co+3.339Ni), and (I) WC-(6.677Co+3.339Ni+6.677Cr) SPS-ed at 1250°C.

Figure 11. FE-SEM micrograph of the cemented carbides of WC-(6.677Co+3.339Ni+6.677Cr) SPS-ed at 1200°C. The image was taken with backscattered electrons for a better distinction between phases (lighter grey is WC, darker grey is β-M(W,C), and black is M_6C).

Figure 12. Lower-magnification FE-SEM micrographs of the cemented carbides of (A) WC-16.693Co, (B) WC-(13.354Co+3.339Ni), and (C) WC-(6.677Co+3.339Ni+6.677Cr) SPS-ed at 1150°C.

Figure 13. (A) Hardness and (B) fracture toughness of the cemented carbides of WC-16.693Co, WC-(13.354Co+3.339Ni), and WC-(6.677Co+3.339Ni+6.677Cr) as a function of the SPS

temperature. Fracture toughness was measured only for the near-fully dense and fully dense cemented carbides.

Figure 14. Friction curves of the cemented carbides of WC-16.693Co, WC-(13.354Co+3.339Ni), and WC-(6.677Co+3.339Ni+6.677Cr) SPS-ed at 1250°C, measured as a function of the sliding distance up to 2000 m.

Figure 15. Optical micrographs of the residual wear tracks in the cemented carbides of WC-16.693Co, WC-(13.354Co+3.339Ni), and WC-(6.677Co+3.339Ni+6.677Cr) SPS-ed at 1250°C, at the conclusion of the wear tests.

Figure 16. FE-SEM micrographs of the residual wear tracks in the cemented carbides of WC-16.693Co, WC-(13.354Co+3.339Ni), and WC-(6.677Co+3.339Ni+6.677Cr) SPS-ed at 1250°C, at the conclusion of the wear tests.

Figure 17. FE-SEM micrographs of particular regions of the residual wear tracks shown in Fig. 15, taken (A) at the edge of the wear track in WC-(6.677Co+3.339Ni+6.677Cr), (B) within the wear track in WC-(6.677Co+3.339Ni+6.677Cr), (C) within the wear track in WC-16.693Co, (D) at the edge of the wear track in WC-(13.354Co+3.339Ni), and (E) within the wear track in WC-16.693Co.

Figure 18. EDS spectra of the cemented carbides of WC-16.693Co, WC-(13.354Co+3.339Ni), and WC-(6.677Co+3.339Ni+6.677Cr) SPS-ed at 1250°C, taken inside the wear tracks, at the edge of the wear tracks, and well outside the wear tracks. Peak assignations are shown only for C, O, and W.

Figure 19. FE-SEM micrographs of the interior of the residual wear tracks shown in Fig. 15, for (A) WC-16.693Co, (B) WC-(13.354Co+3.339Ni), and (C) WC-(6.677Co+3.339Ni+6.677Cr)).

Figure 20. Higher-magnification FE-SEM micrographs of the interior of the residual wear tracks shown in Fig. 15, displaying details of grooves for (A) and (B) WC-16.693Co, and (C) WC-(13.354Co+3.339Ni). The arrows in (A) are to facilitate the observation of the thin tribolayer.

Table 1. Designation and composition of the three types of cemented carbides fabricated in this study.

Designation	Desired cemented carbide				Powder batch (wt.%)			
	WC+binder (vol.%)	Metal binder (vol.% of the total)			WC	Co	Ni	Co
		Co	Ni	Cr				
WC-16.693Co	83.307+16.693	100	0	0	90	10	0	0
WC-(13.354Co+3.339Ni)	83.307+16.693	80	20	0	89.979	7.998	2.023	0
WC-(6.677Co+3.339Ni+6.677Cr)	83.307+16.693	40	20	40	90.646	4.029	2.038	3.287

Figure

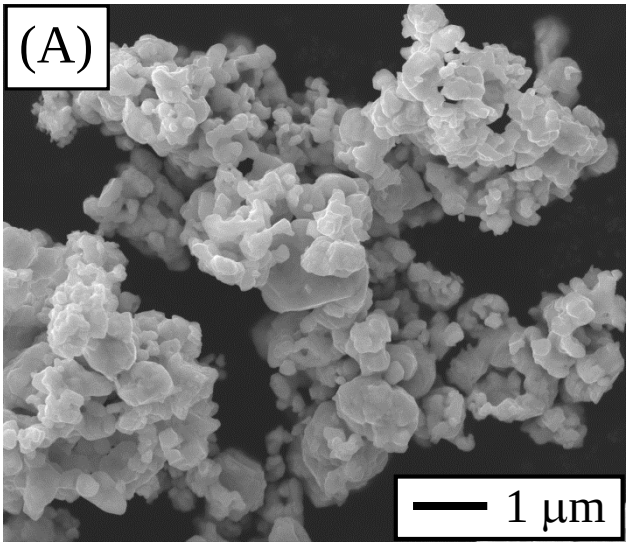

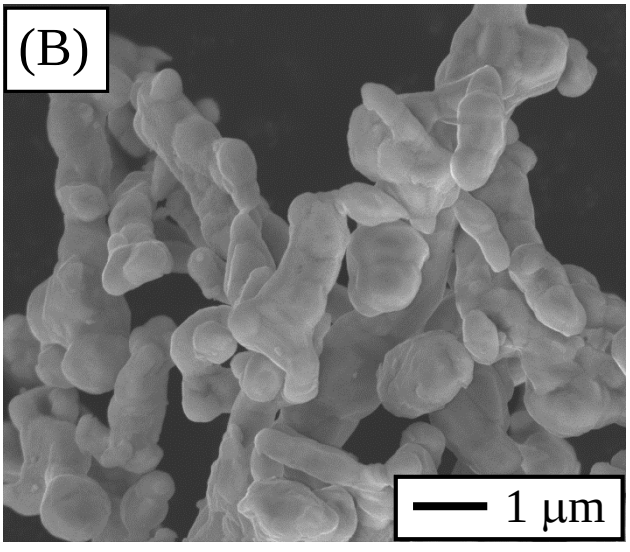

Boukantar *et al.*
Figure 1

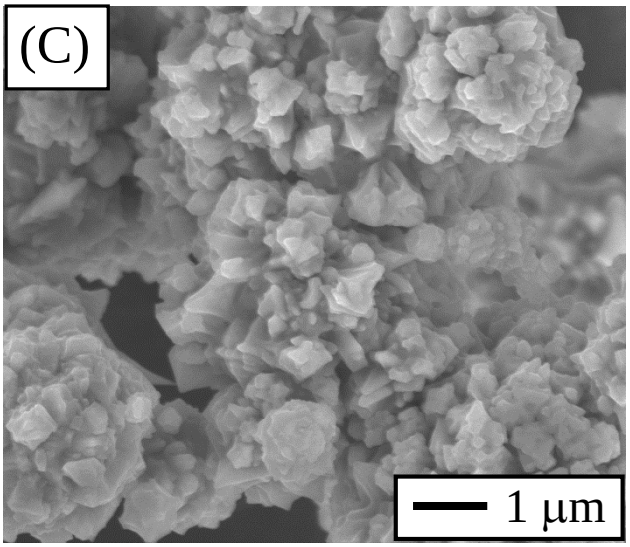

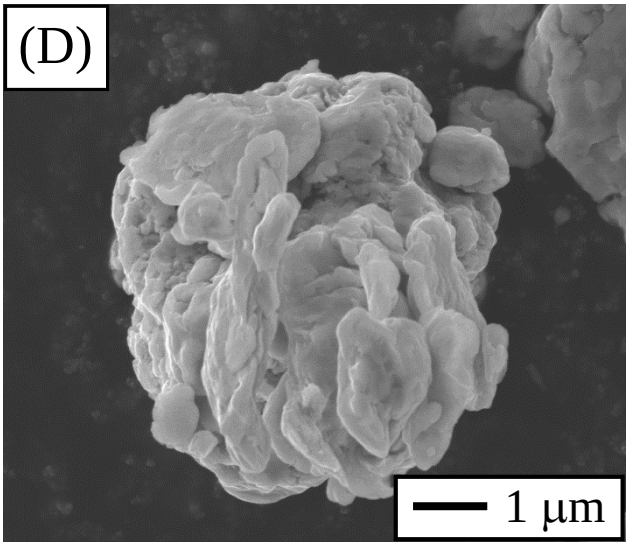

Boukantar *et al.*
Figure 1

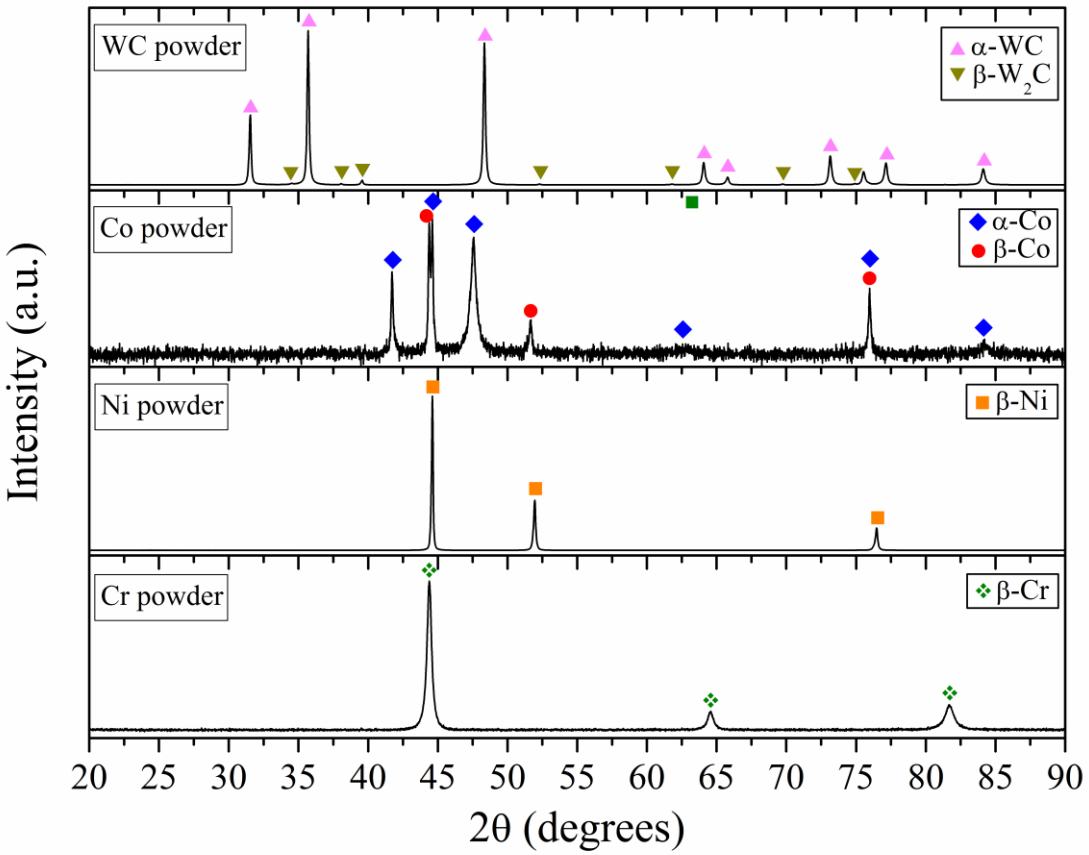

Boukantar *et al.*
Figure 2

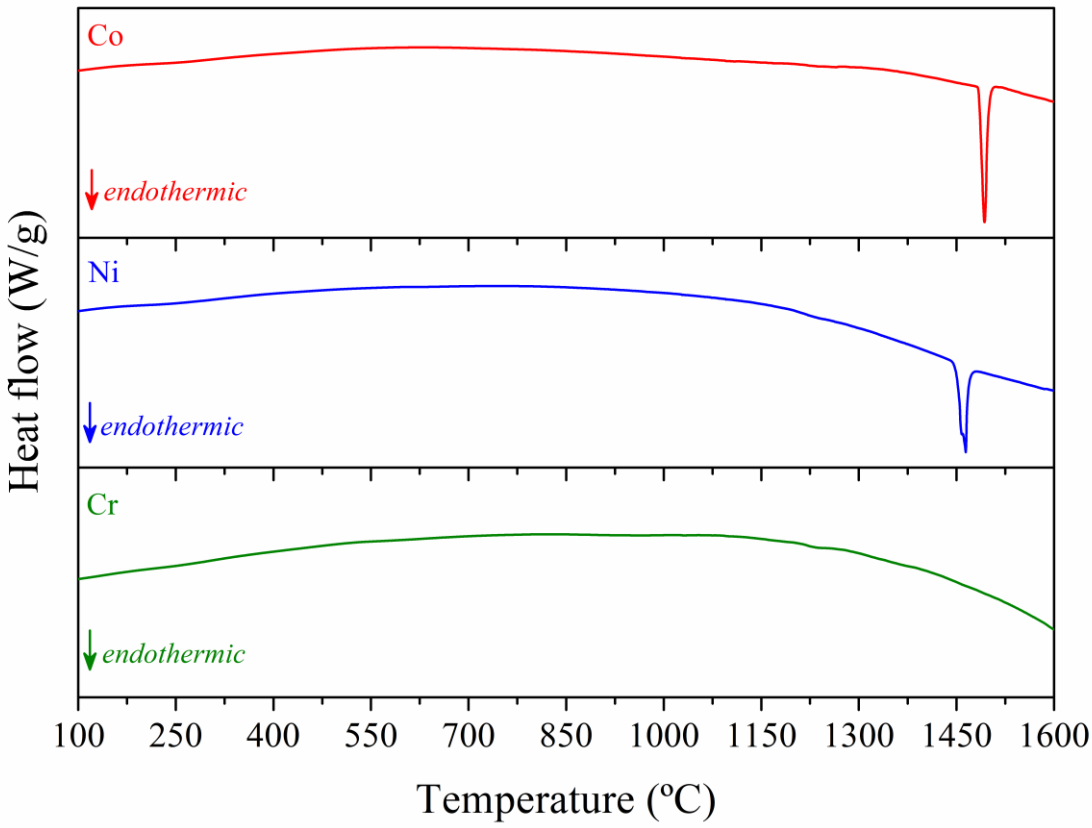

Boukantar *et al.*
Figure 3

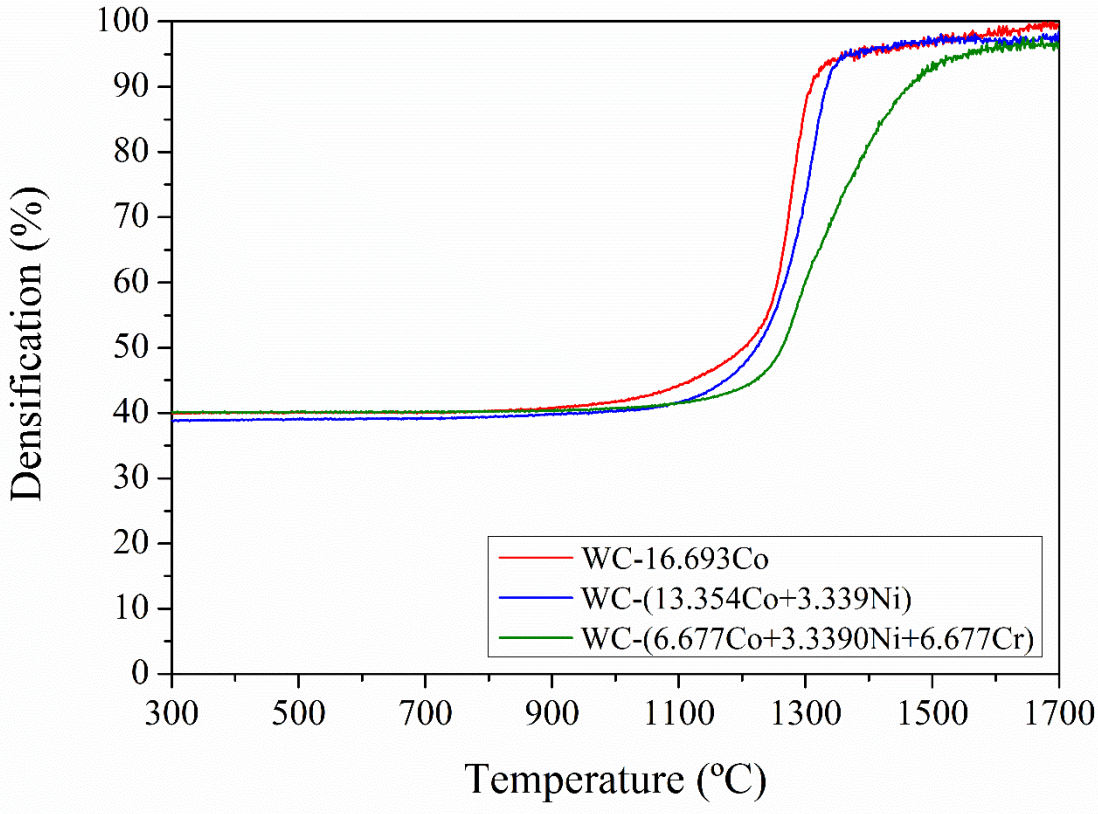

Boukantar *et al.*
Figure 4

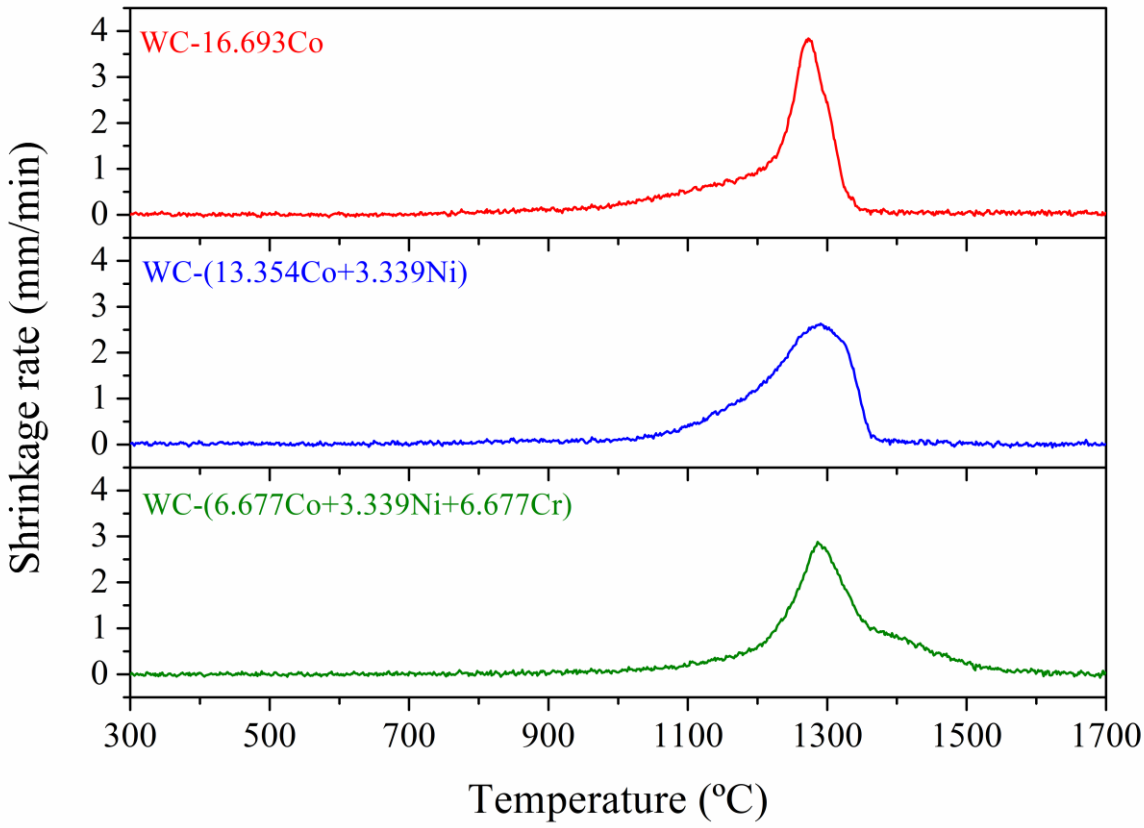

Boukantar *et al.*
Figure 5

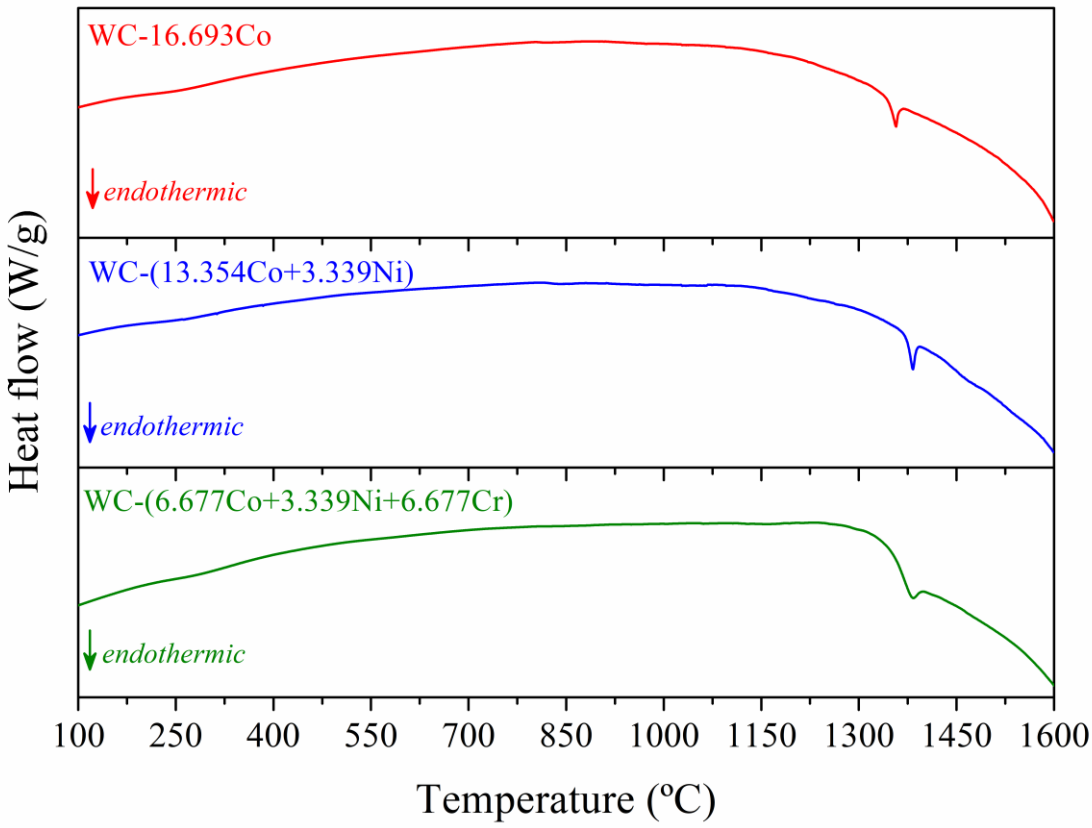

Boukantar *et al.*
Figure 6

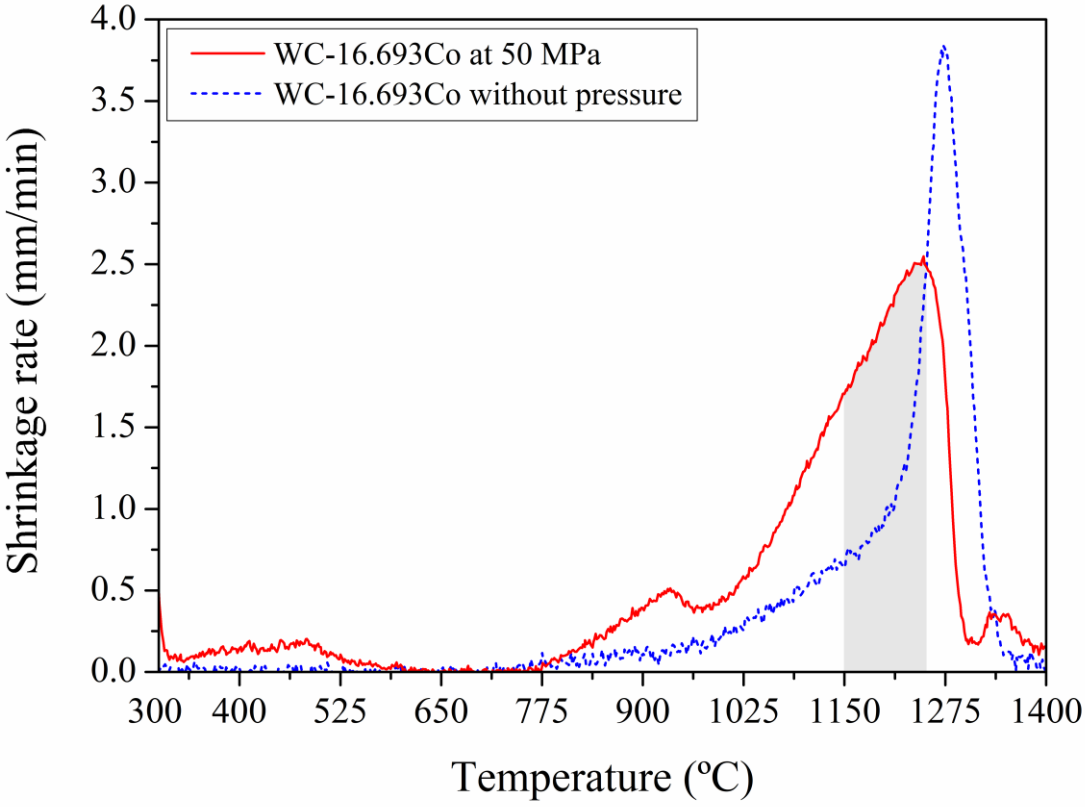

Boukantar *et al.*
Figure 7

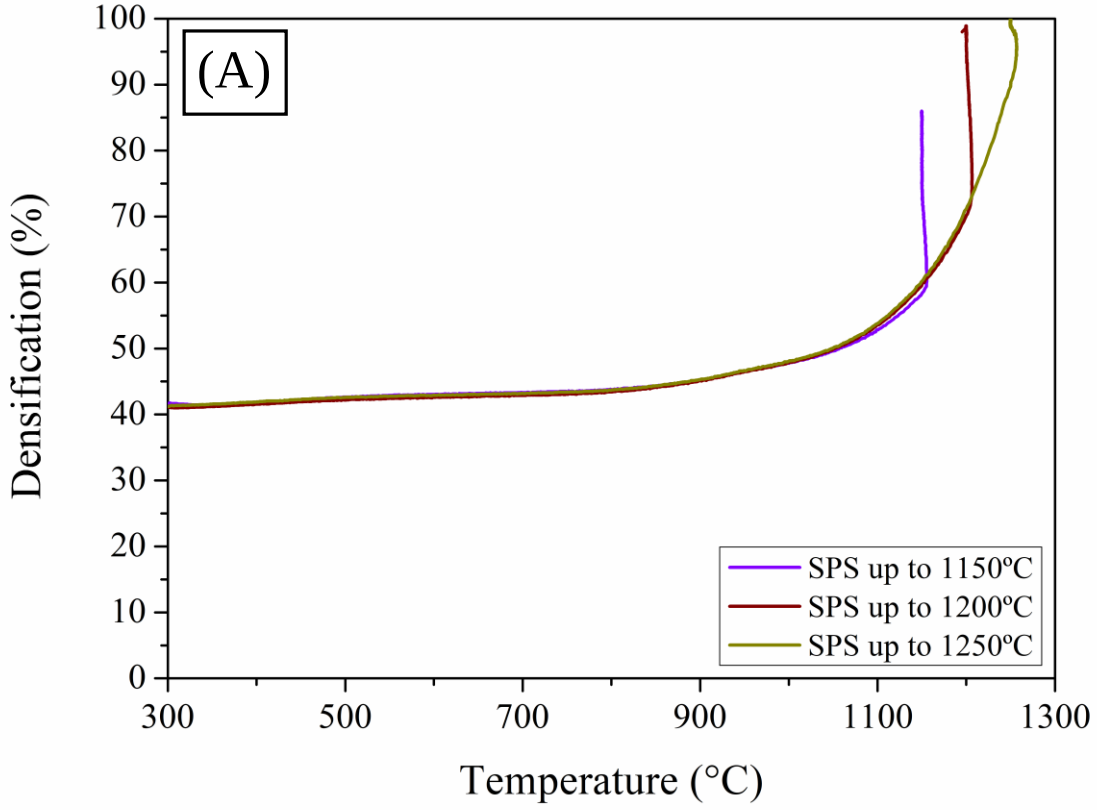

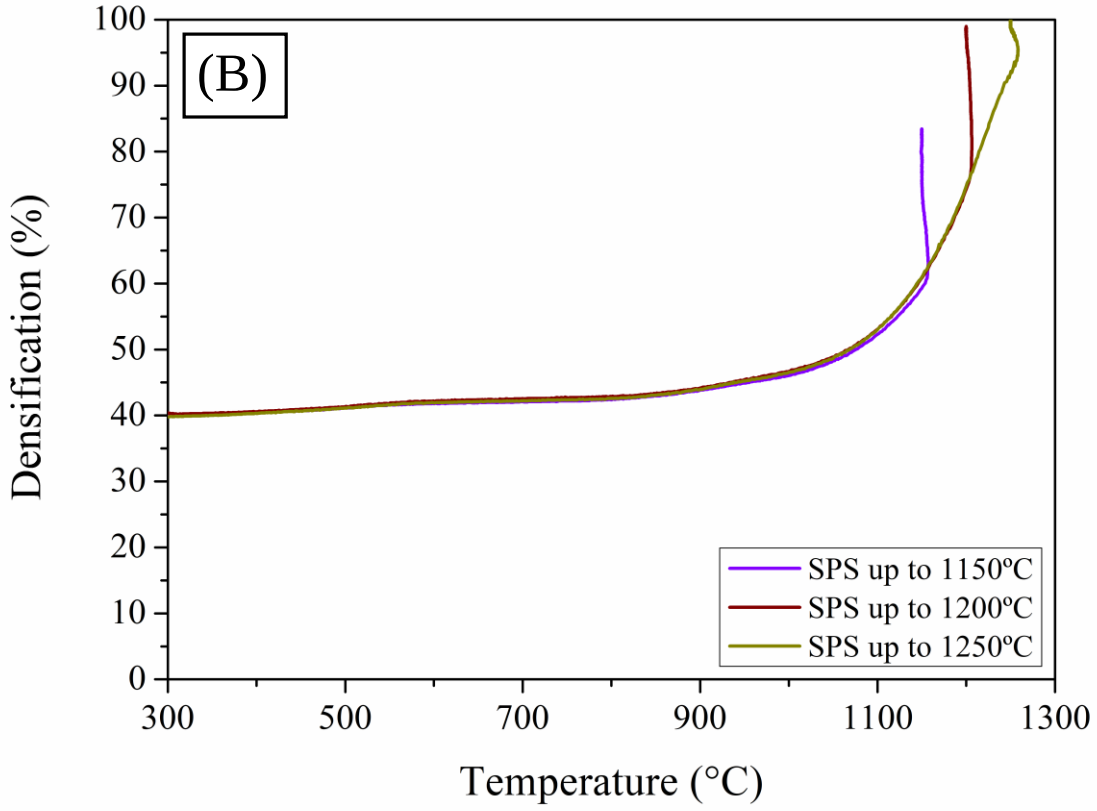

Boukantar *et al.*
Figure 8

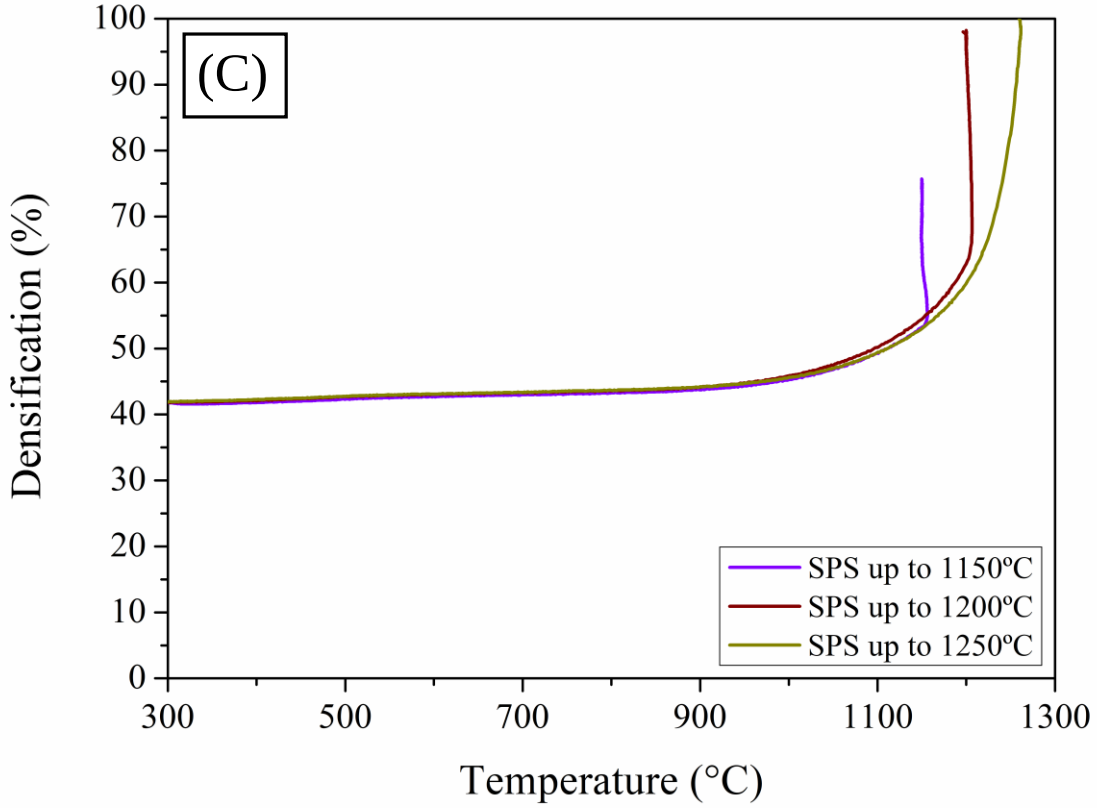

Boukantar *et al.*
Figure 8

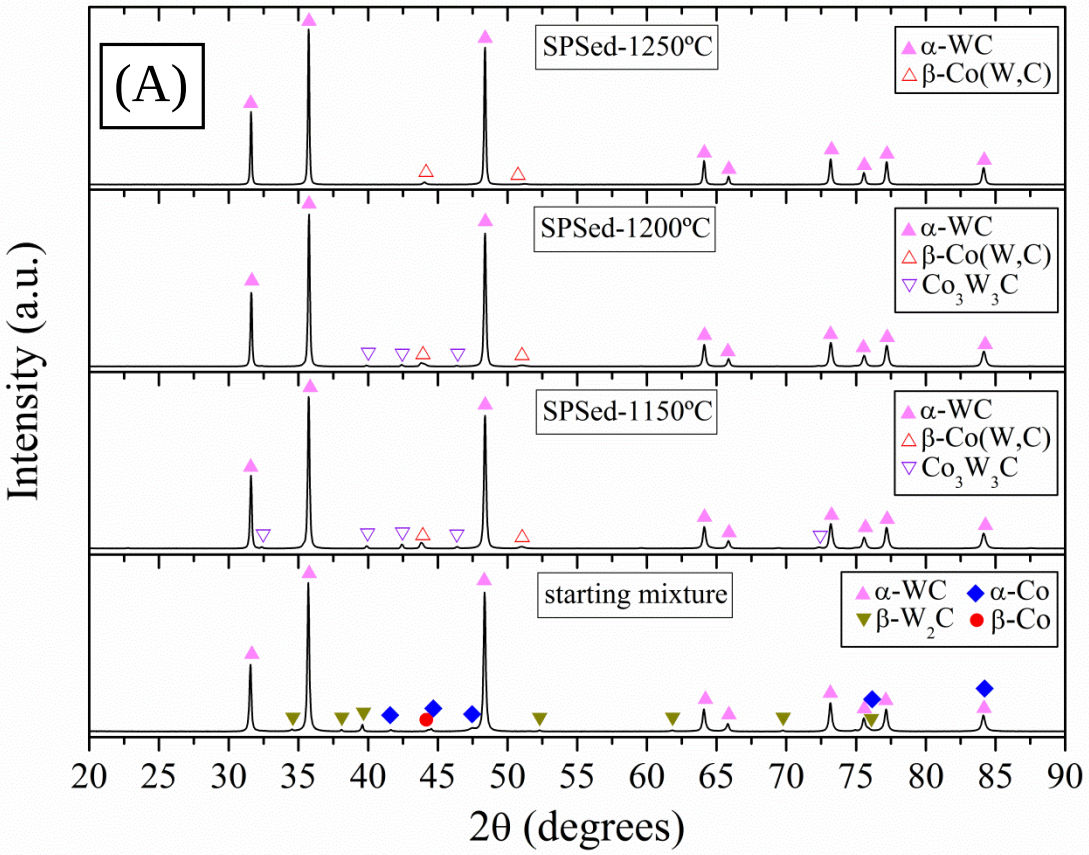

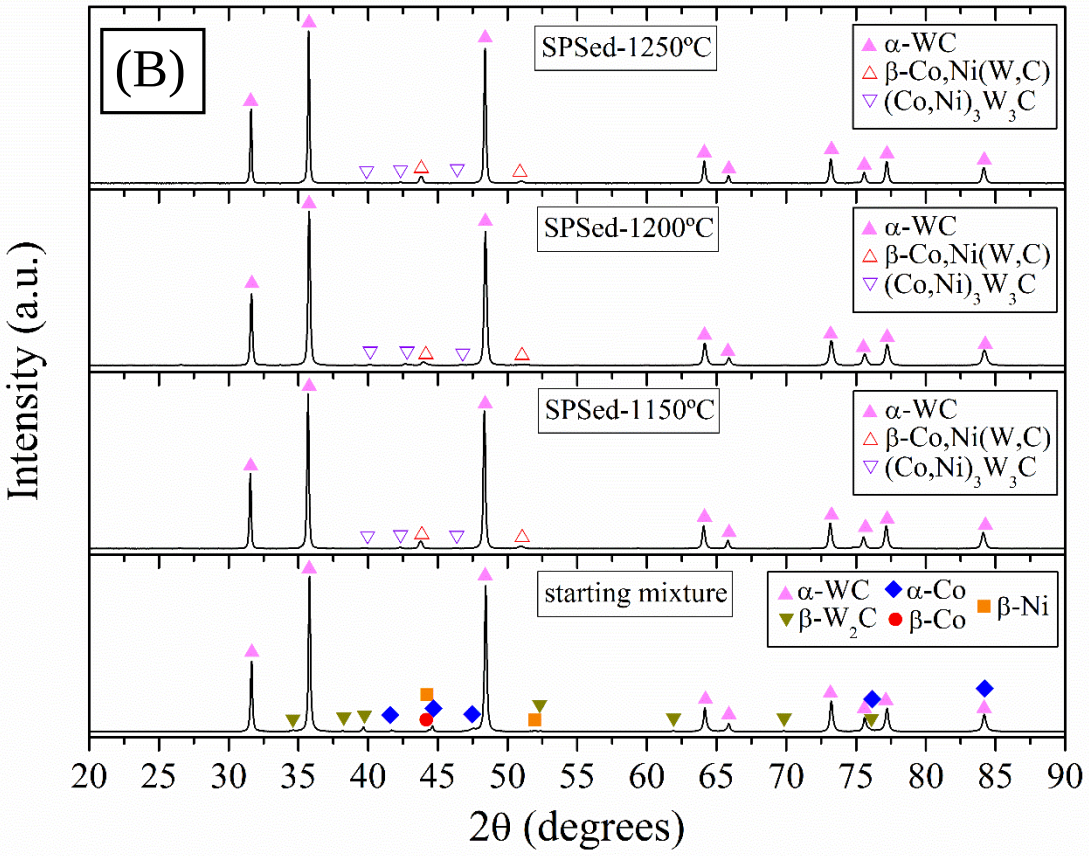

Boukantar *et al.*
Figure 9

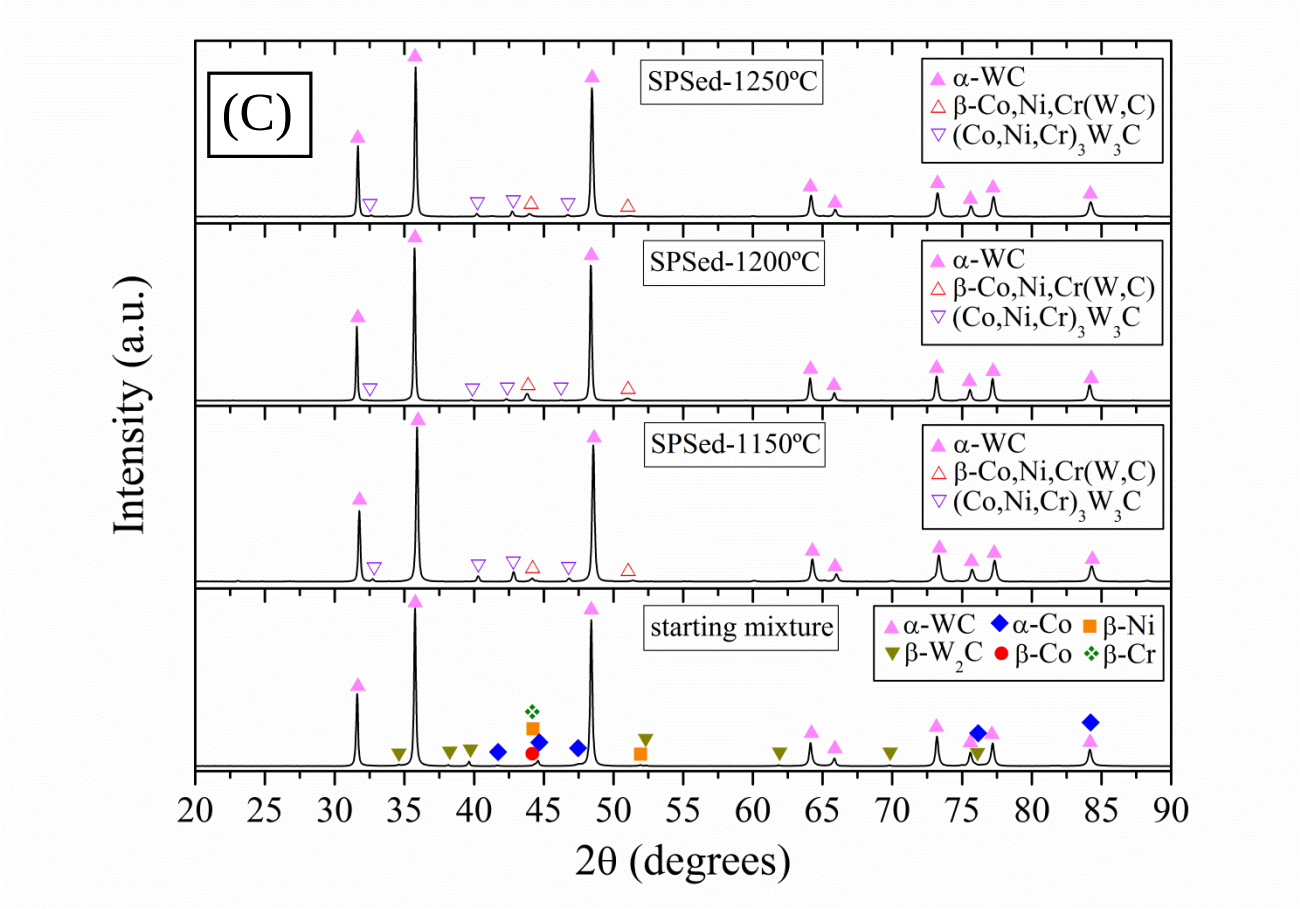

Boukantar *et al.*
Figure 9

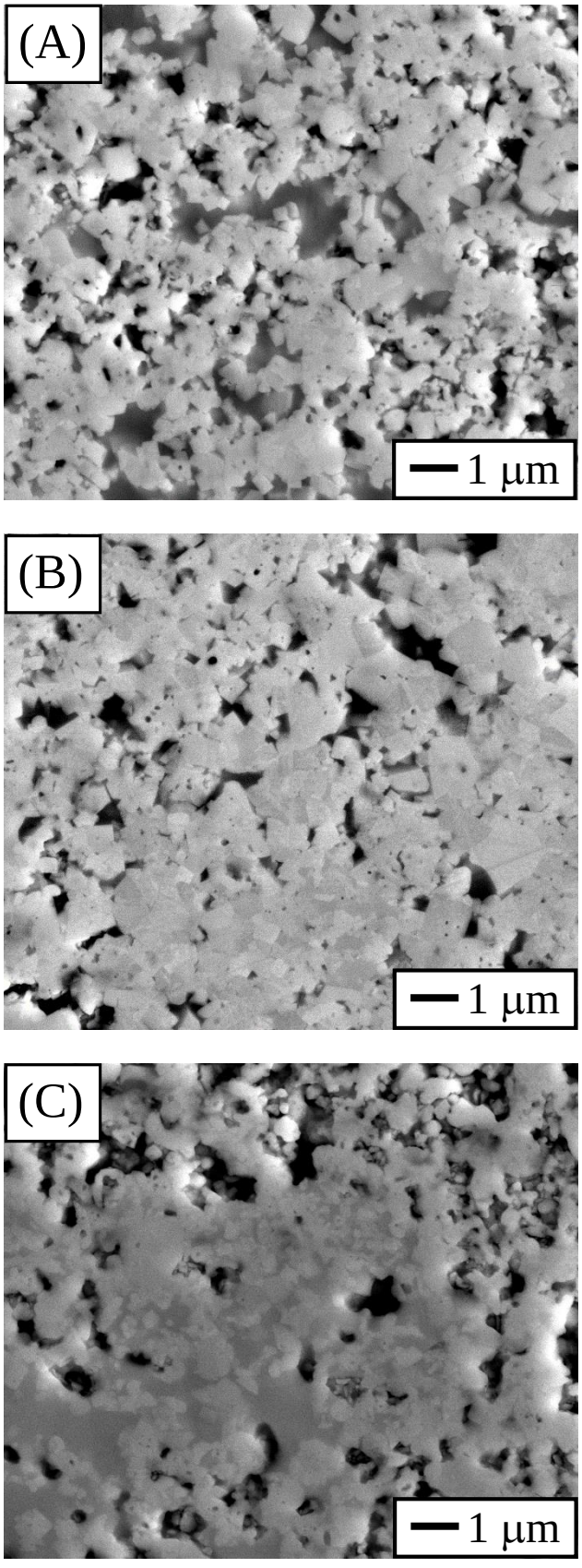

Boukantar *et al.*
Figure 10

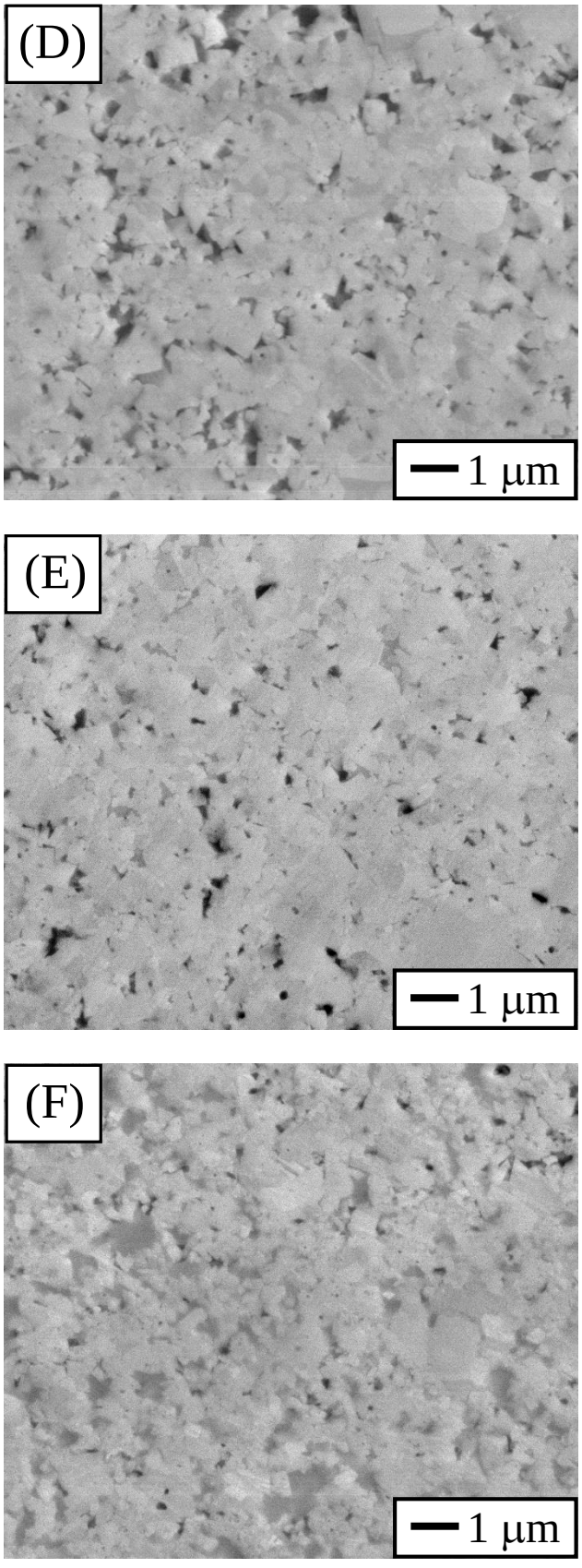

Boukantar *et al.*
Figure 10

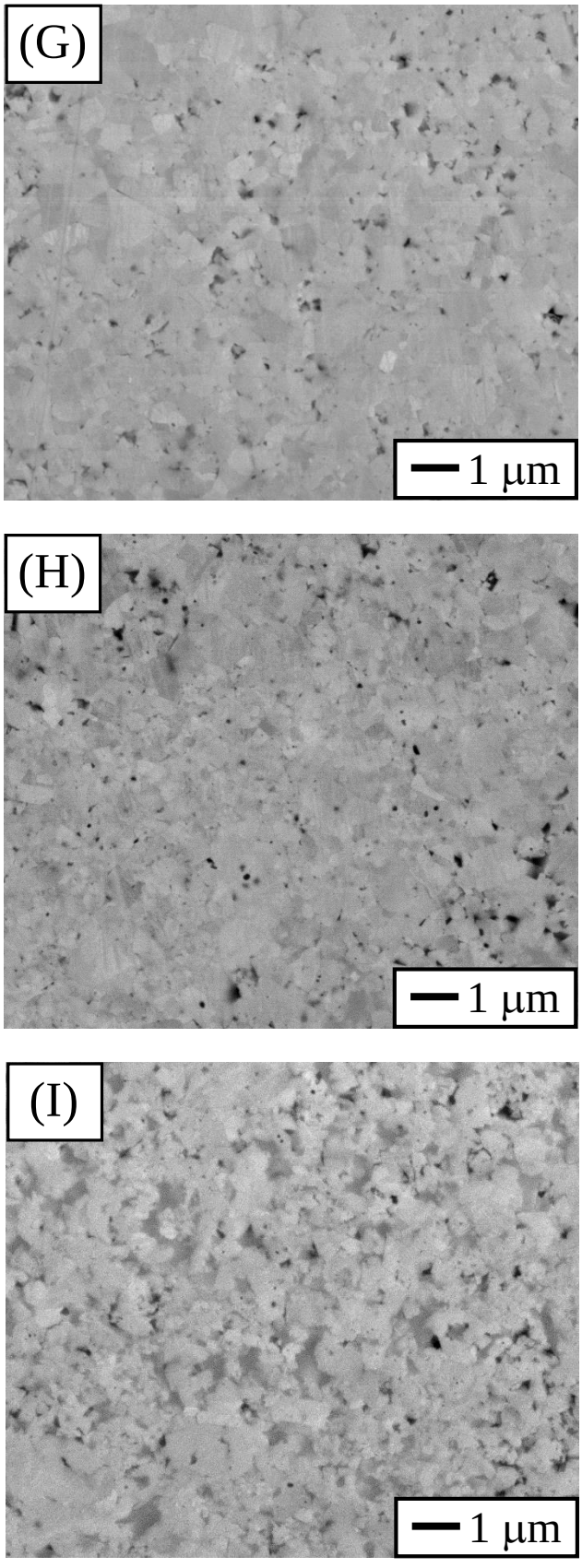

Boukantar *et al.*
Figure 10

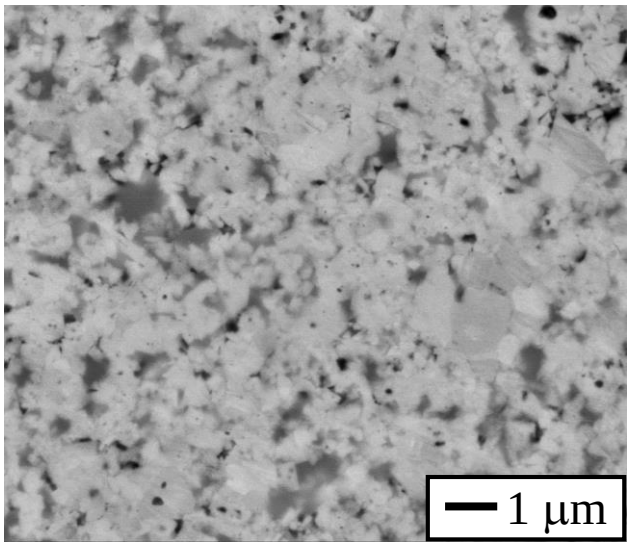

Boukantar *et al.*
Figure 11

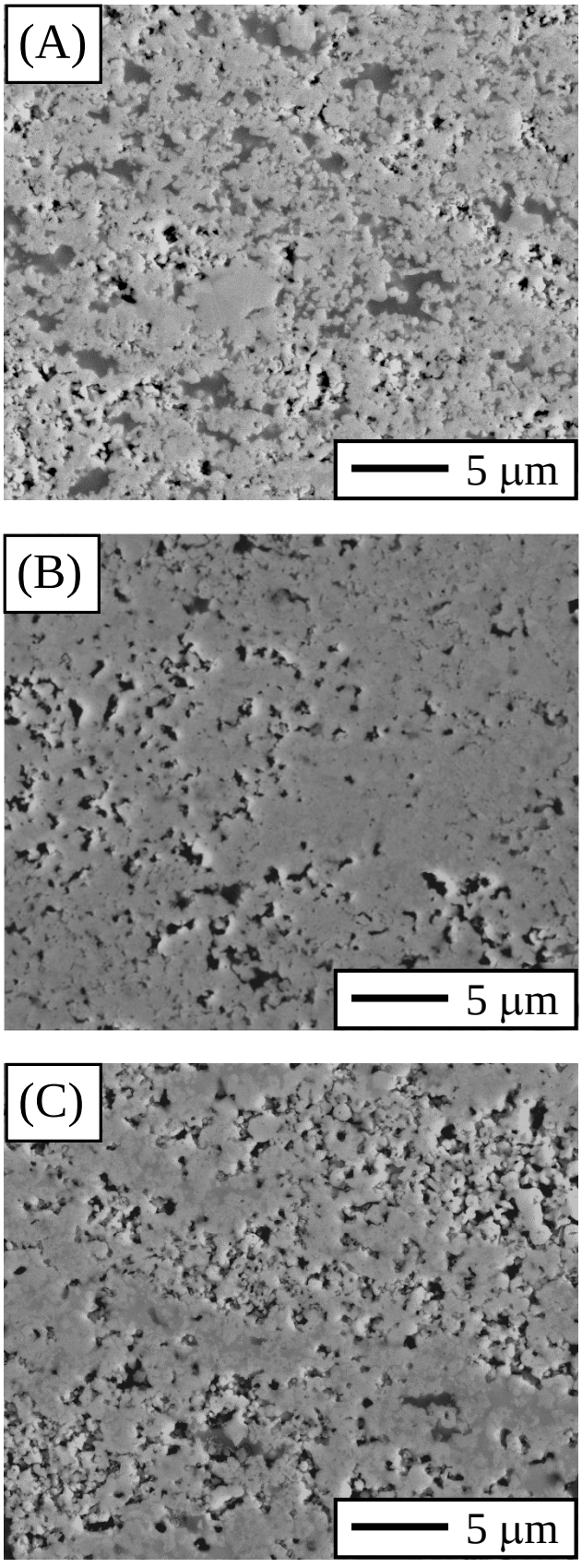

Boukantar *et al.*
Figure 12

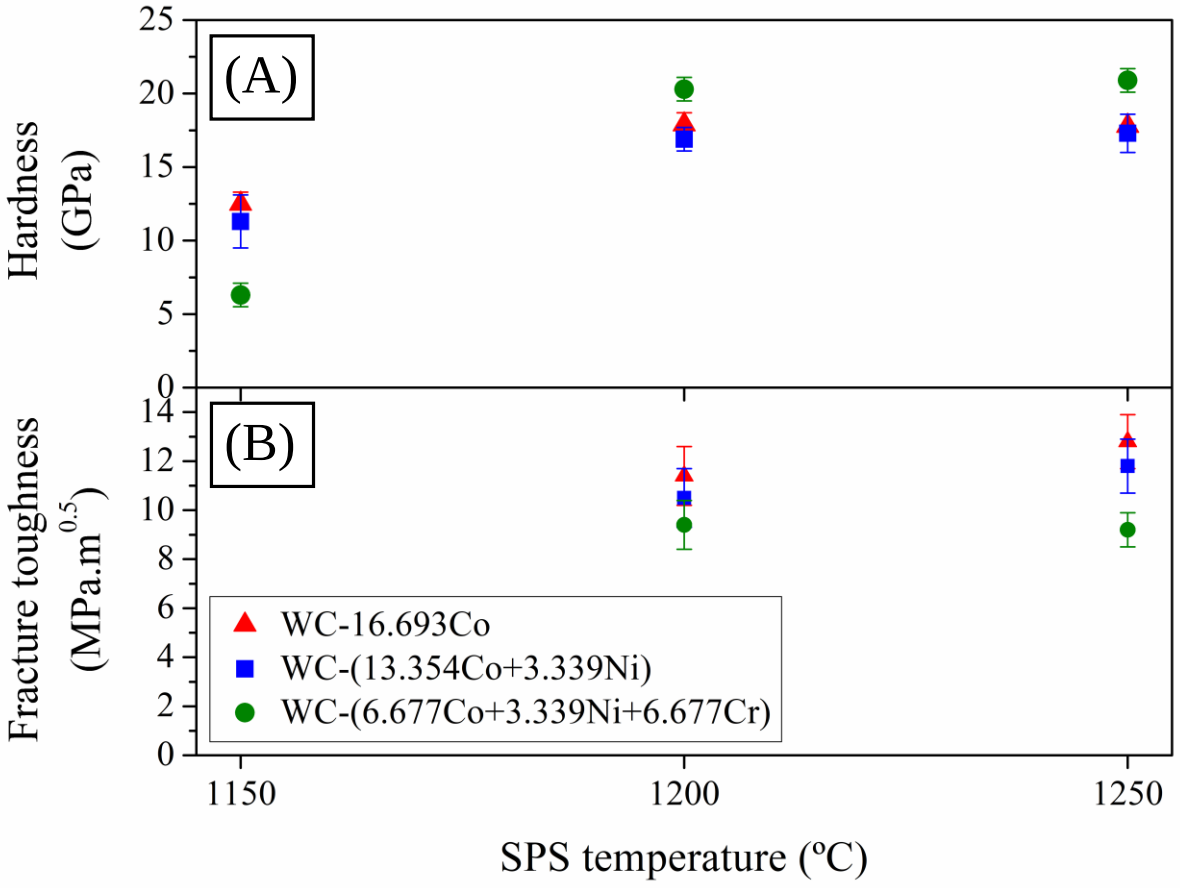

Boukantar *et al.*
Figure 13

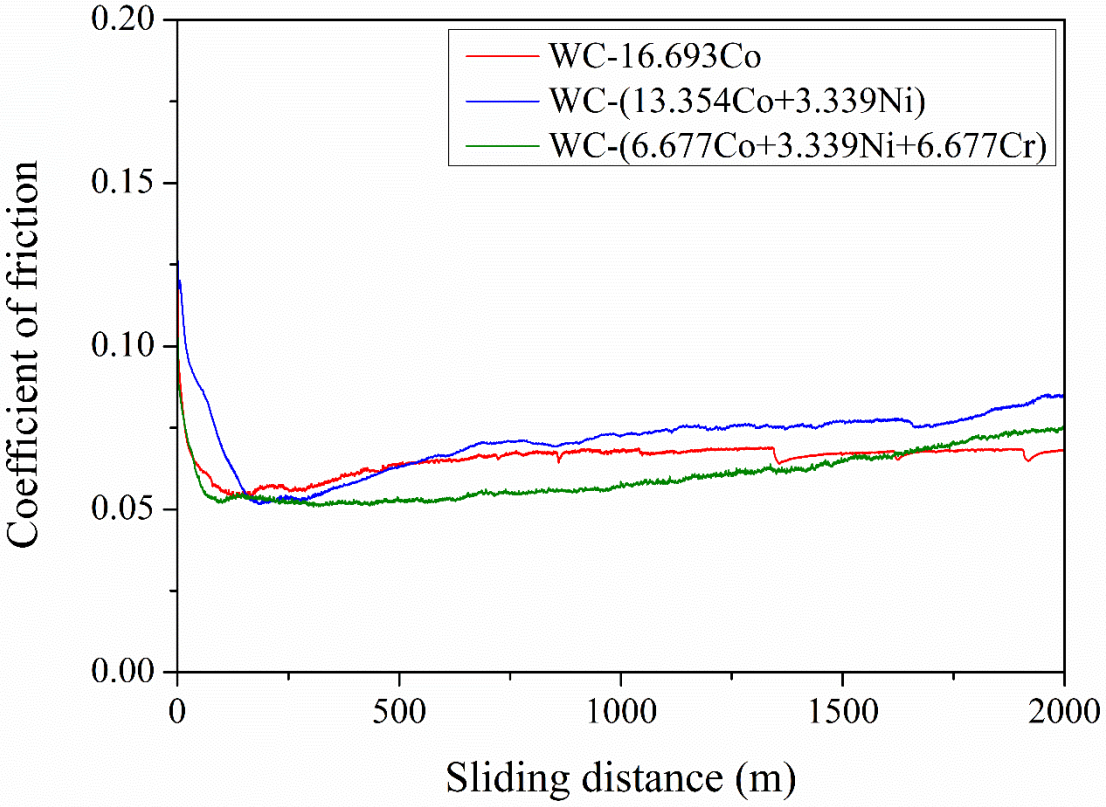

Boukantar *et al.*
Figure 14

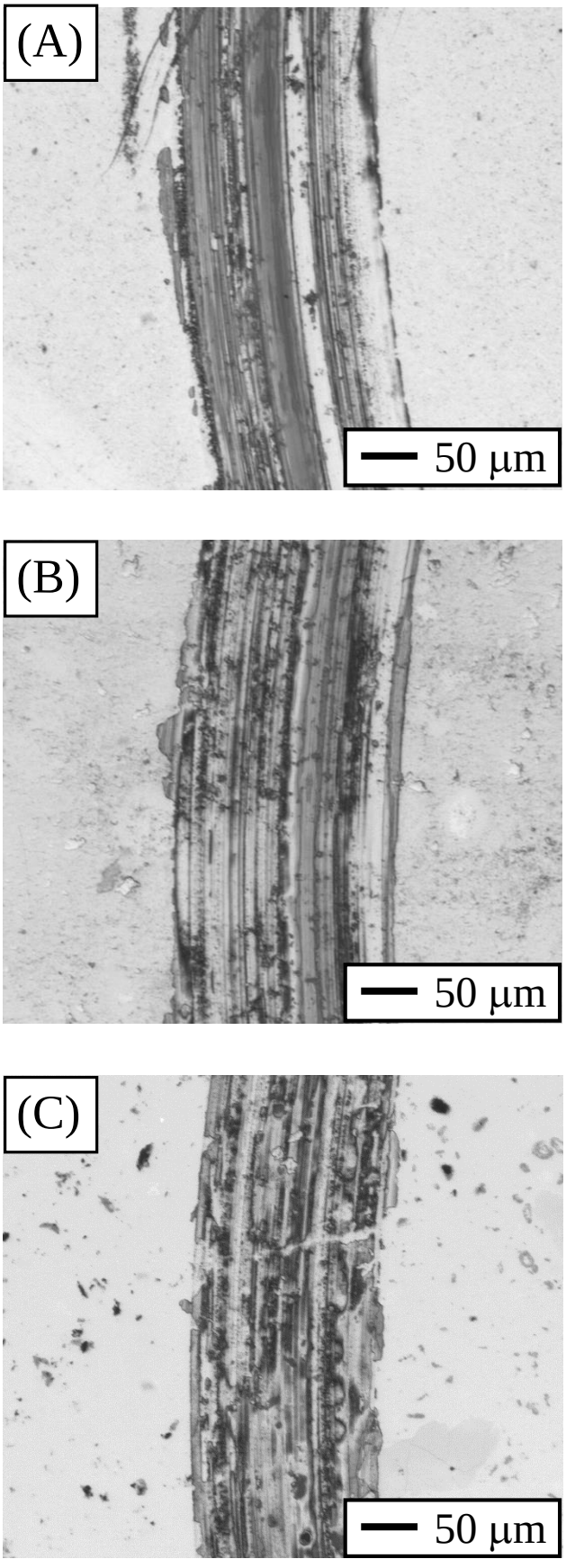

Boukantar *et al.*
Figure 15

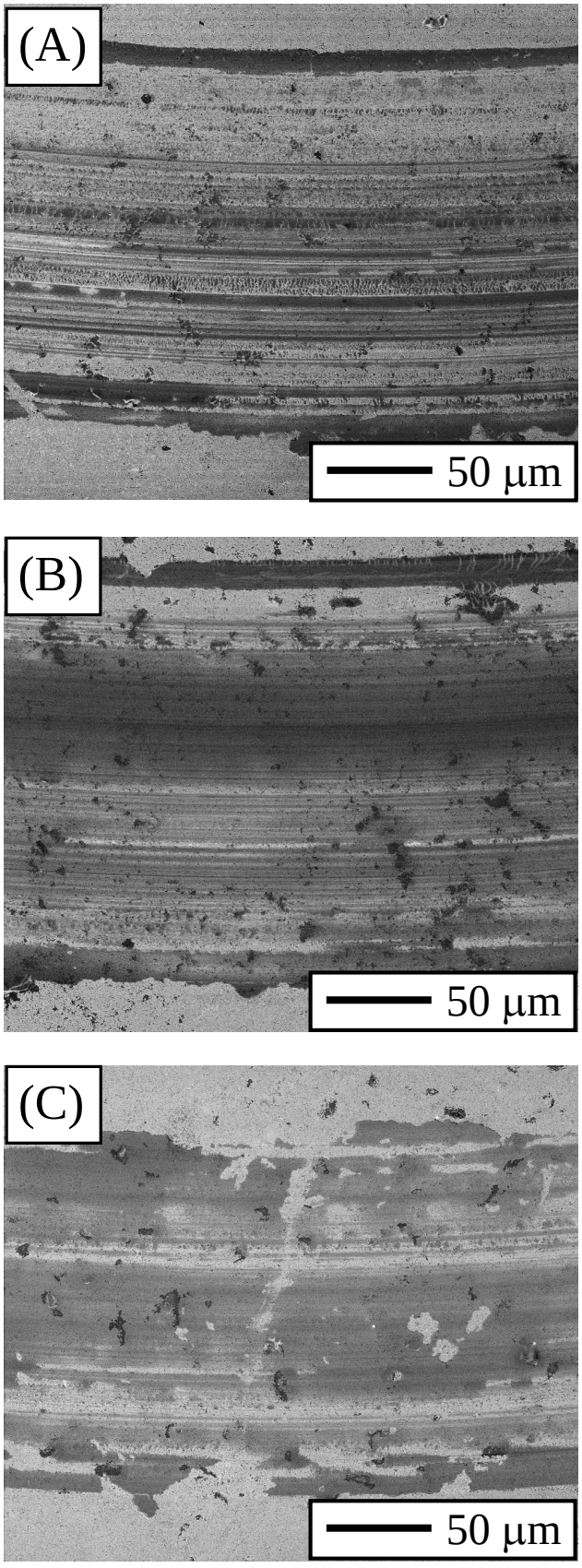

Boukantar *et al.*
Figure 16

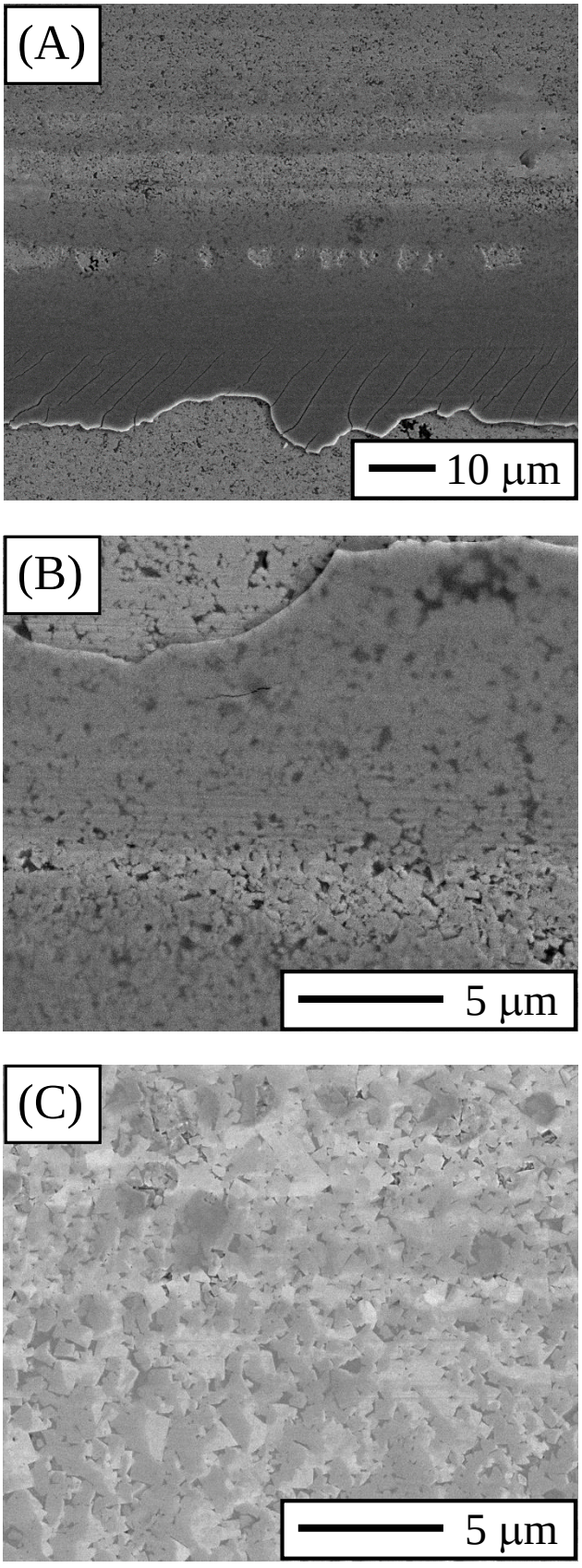

Boukantar *et al.*
Figure 17

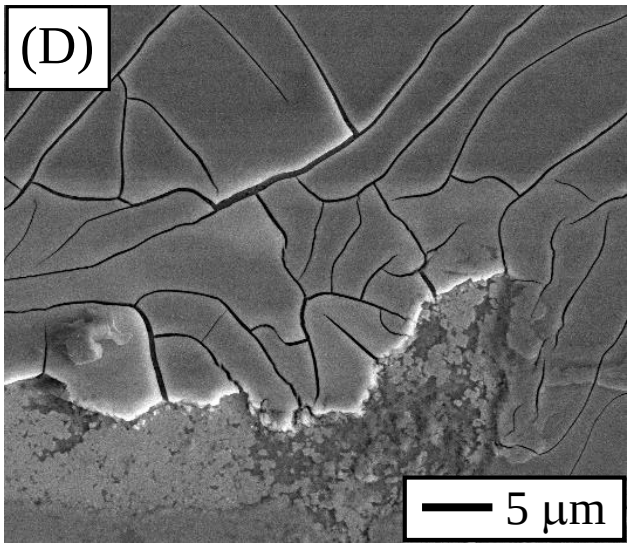

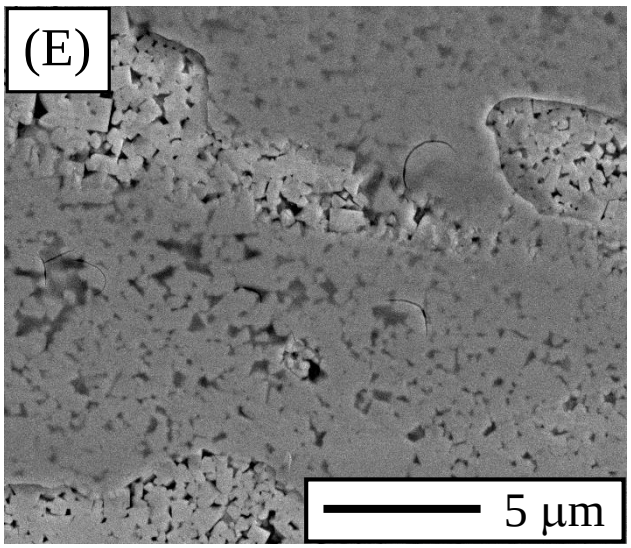

Boukantar *et al.*
Figure 17

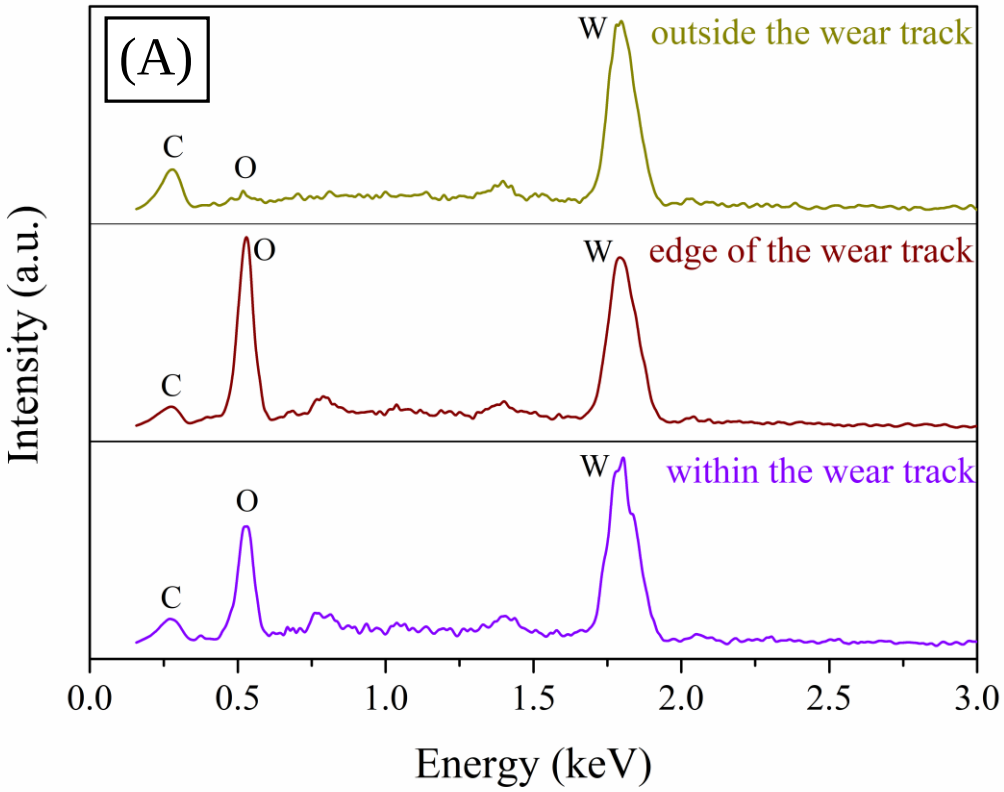

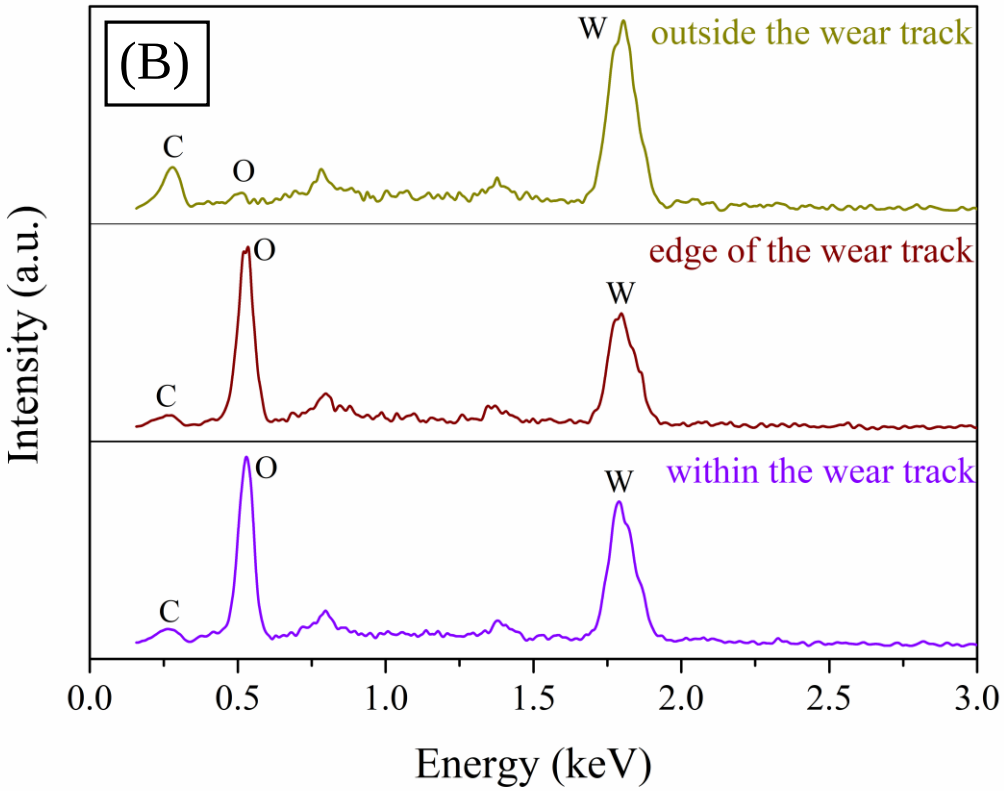

Boukantar *et al.*
Figure 18

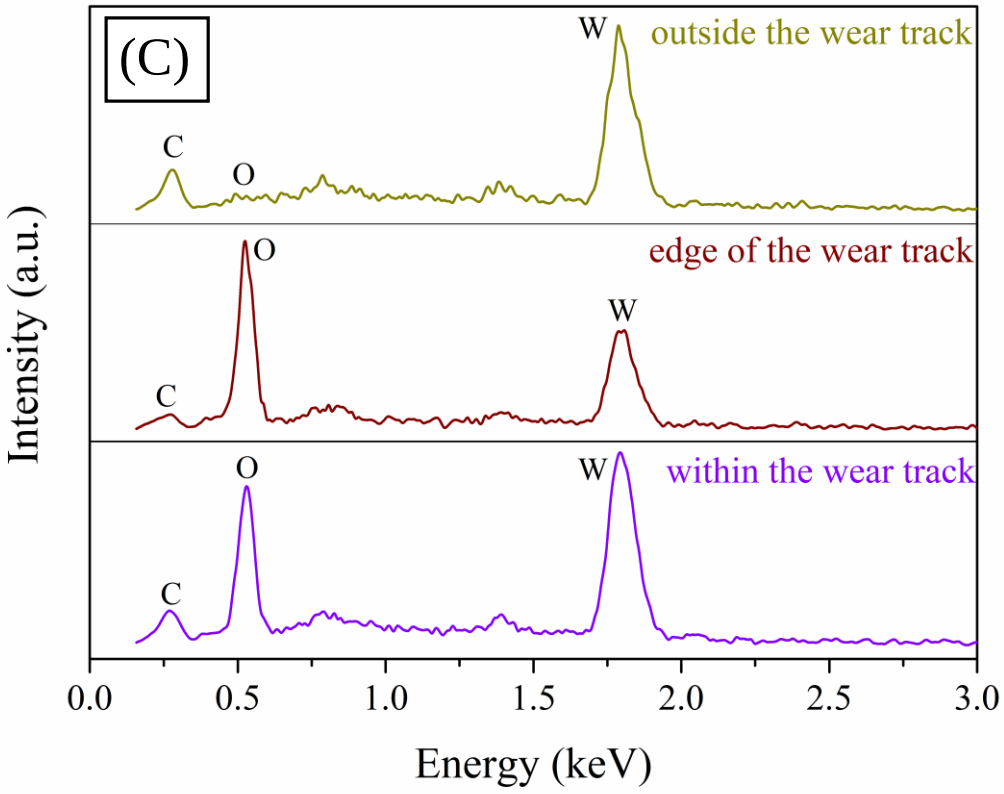

Boukantar *et al.*
Figure 18

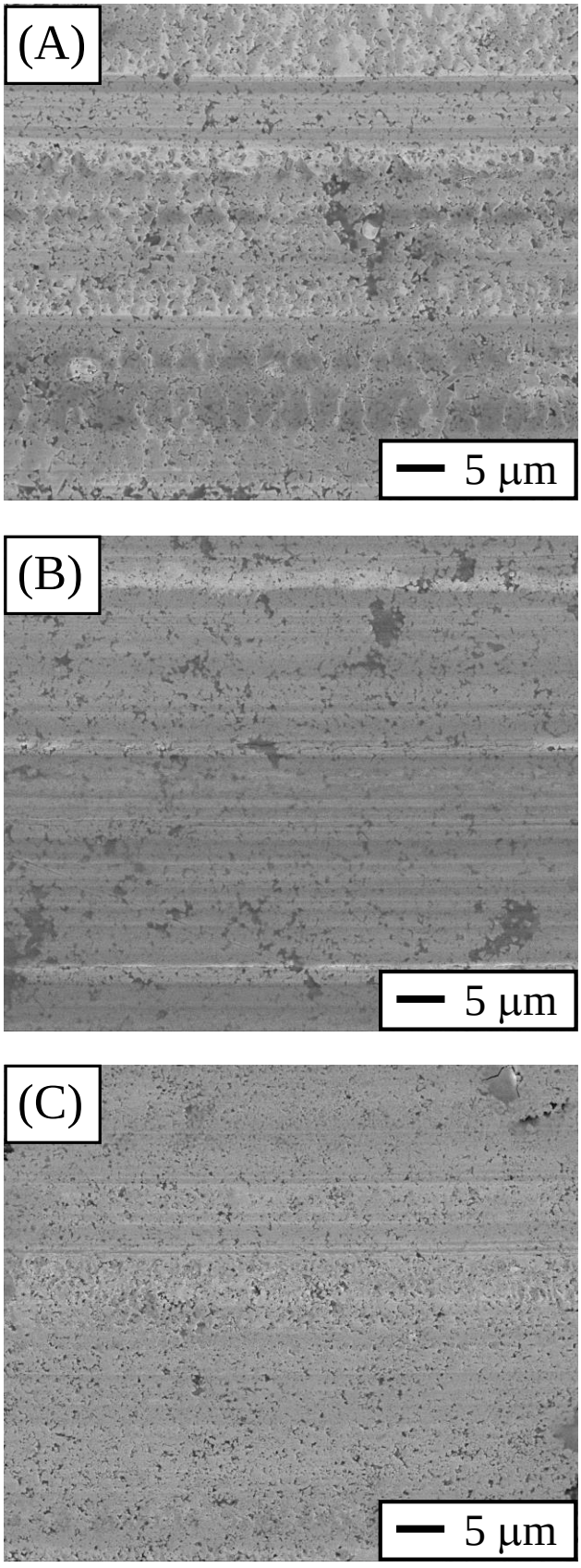

Boukantar *et al.*
Figure 19

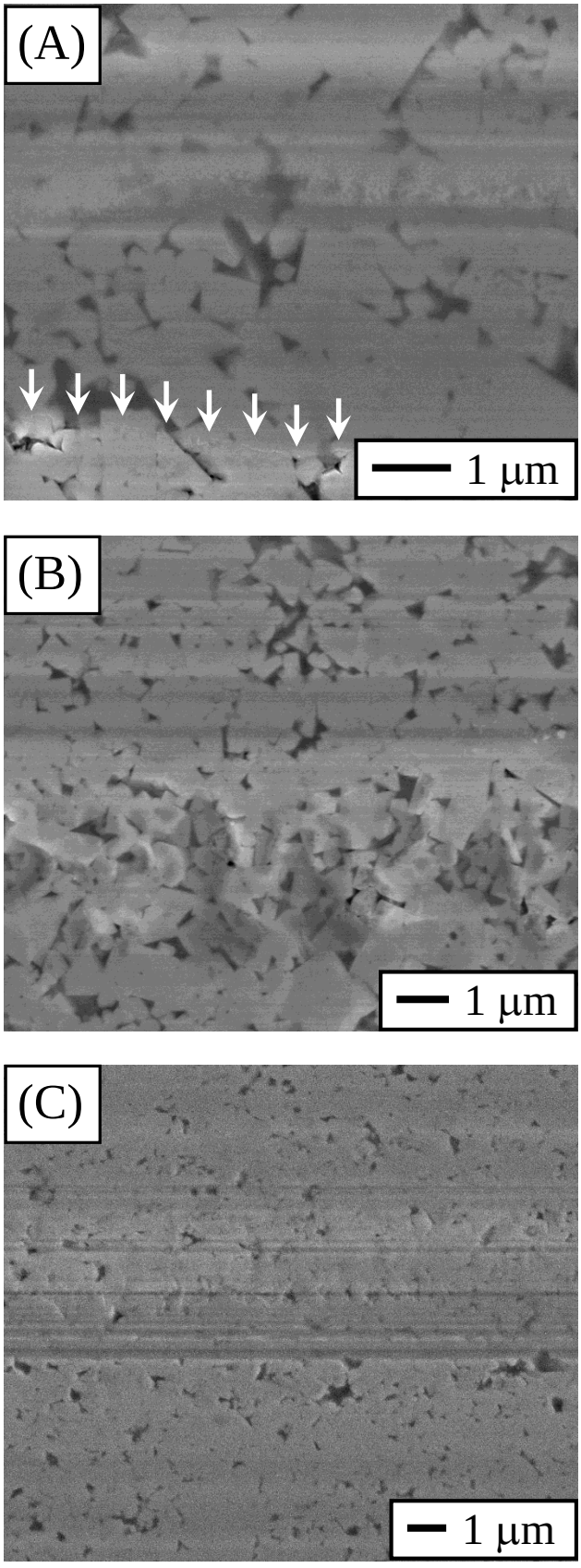

Boukantar *et al.*
Figure 20

Author contributions

Aniss-Rabah Boukantar decided the research topic, discussed the research plan, collected the relevant bibliography, performed most experiments, analyzed data, discussed results and analyses, contributed to writing the manuscript, and revised the manuscript. Boubekeur Djerdjare decided the research topic, discussed the research plan, and revised the manuscript. Fernando Guiberteau discussed the research plan, debated results and analyses, and revised the manuscript. Angel L. Ortiz discussed the research plan, designed the study, performed some experiments, analyzed data, discussed results and analyses, and wrote the manuscript.

- A critical comparison has been made between the spark-plasma sinterability and dry sliding-wear resistance of WC densified with Co, Co+Ni, and Co+Ni+Cr.
- Partial substitutions of Co by Ni and by Ni+Cr reduce (slightly the former and considerably the latter) the pressureless ultrafast sinterability of WC, attributable to the greater temperatures required for the formation of low-viscosity eutectic liquid.
- The metal binder (Co, Co+Ni, or Co+Ni+Cr) does not condition the ultrafast sinterability under the typical pressures applied in conventional SPS.
- WC-(Co+Ni+Cr) is markedly harder than both WC-Co and WC-(Co+Ni), while still preserving a high fracture toughness, which is a good combination of mechanical properties for very many structural applications.
- WC-(Co+Ni+Cr) has excellent intrinsic dry sliding-wear resistance that comparatively exceeds those of WC-Co and WC-(Co+Ni) by a factor of two.
- Wear of these cemented carbides under dry sliding contact in air occurs principally by two-body abrasion dominated by plastic deformation, with some oxidative wear.